Application of Genetic Algorithms to the Solution of the Space Vehicle Reentry Trajectory Optimization Problem

Jean-Antoine Desideri, Sergey Peigin, Sergey Timchenko

INRIA

INSTITUT NATIONAL DE RECHERCHE EN INFORMATIQUE ET EN AUTOMATIQUE

Application of Genetic Algorithms to the Solution of the Space Vehicle Reentry Trajectory Optimization Problem

Jean-Antoine Désidéri, Sergey Peigin and Sergey Timchenko

N° 3843

Décembre 1999

THÈME 4

ISSN 0249-6399 ISRN INRIA/RR--3843--FR+ENG

INRIA
SOPHIA ANTIPOLIS

Application of Genetic Algorithms to the Solution of the Space Vehicle Reentry Trajectory Optimization Problem

Jean-Antoine Désidéri*, Sergey Peigin† and Sergey Timchenko‡

Thème 4 — Simulation et optimisation
de systèmes complexes
Projet Sinus

Rapport de recherche n° 3843 — Décembre 1999 — 42 pages

Abstract: During the atmospheric reentry of a space vehicle the heat flux at the body surface is so large that one has to solve a very complex heat protection problem for the space vehicle surface. One of the possible passive ways to reduce the heat flux at the body surface is to optimize the reentry trajectory parameters to minimize of the heat flux integral. The purpose of this report is to solve the optimization problem of the reentry trajectory into the Earth atmosphere with respect to the heat flux integral at the stagnation point of 3D blunt body. This problem is solved by means of the floating-point Genetic Algorithms (GA) via calculation of the heat flux evolution along the reentry trajectory in the framework of the non-equilibrium multicomponent thin viscous shock layer model (TVSL). The solution of this problem by Genetic Algorithms is interesting from both practical applicative and methodological points of view, because it is a very good example to demonstrate the GA efficiency for the solution of an optimization problem with a number of complex non-linear constraints. The influence of the GA parameters as well as the body

* INRIA, 2004 Route des Lucioles, BP. 93, 06902 Sophia Antipolis Cédex-France
† TECHNION, Technion City, 32000, Haifa, Israel
‡ Tomsk University, 634050, Lenina 36, Tomsk, GSP-14, Russia

Unité de recherche INRIA Sophia Antipolis
2004, route des Lucioles, B.P. 93, 06902 Sophia Antipolis Cedex (France)
Téléphone : 04 92 38 77 77 - International : +33 4 92 38 77 77 — Fax : 04 92 38 77 65 - International : +33 4 92 38 77 65

geometry, the body surface catalytic activity and certain physical constraints on the optimum solution and on the algorithm arithmetical cost efficiency is investigated.

Key-words: GA, TVSL, heat flux, trajectory optimization, non-linear constraints

Application d'algorithmes génétiques à l'optimisation de la trajectoire de rentrée d'un véhicule spatial

Résumé : Dans la phase de rentrée atmosphérique d'un véhicule spatial, l'importance du transfert thermique pariétal rend nécessaire la résolution du problème complexe de la protection thermique. Un moyen passif de réduire le flux de chaleur pariétal consiste à optimiser les paramètres de la trajectoire afin de minimiser l'intégrale en temps du flux de chaleur. Le but de ce rapport est de résoudre le problème de l'optimisation de la trajectoire de rentrée atmosphérique vis à vis de l'intégrale du flux au point d'arrêt d'un corps arrondi tridimensionnel. Ce problème est résolu par un algorithme génétique (AG) en codage réel par le biais du calcul de l'évolution du flux thermique au cours de la trajectoire en faisant l'hypothèse d'un écoulement de fluide réactif hors-équilibre chimique et de couche de choc visqueuse mince (modèle TVSL, *thin viscous shock layer*). La résolution de ce problème par algorithme génétique présente un intérêt applicatif mais aussi méthodologique, car il s'agit d'un très bon exemple démonstratif de l'efficacité de l'AG à résoudre un problème d'optimisation soumis à de nombreuses contraintes nonlinéaires. L'influence des paramètres de définition de l'AG ainsi que la géométrie du corps, le degré d'activité catalytique de la surface et certaines contraintes physiques sur la solution optimale et le coût de l'algorithme est évaluée.

Mots-clés : AG, TVSL, flux thermique, optimisation de trajectoire, contraintes nonlinéaires

Contents

1 INTRODUCTION

It is well-known that during the space vehicle reentry into the Earth atmosphere the heat flux at the body surface is so large that one has to solve a very complex heat protection problem for the vehicle surface. One of the possible passive ways to reduce the heat flux at the body surface is to optimize the reentry trajectory parameters to minimize the heat flux integral. In this case the solution of the heat flux optimization aerospace design problem is presented in this report.

This problem is the problem of the reentry trajectory optimization into the Earth atmosphere with respect to the integral of the heat flux at the stagnation point of a 3D blunt body. This optimization problem is solved with the physical constraints on the body acceleration along trajectory and on the maximum value of equilibrium temperature of the body surface - the maximum equilibrium temperature of the body surface T_w cannot exceed a preassigned limit value T_w^{max}.

As an objective function, the integral convective heat flux Q' at the body surface along the full trajectory is considered and the value Q' is computed on the basis of the numerical solution of the multicomponent nonequilibrium thin viscous shock layer equations (TVSL).

To solve this problem a variant of the robust floating-point Genetic Algorithms is used with the arithmetical crossover operator and with the nonuniform distance-dependent mutation operator.

2 PROBLEM STATEMENT

Let us consider the space vehicle moving along trajectory into the Earth atmosphere. The vehicle reentry is beginning from the altitude $H_0 = 100km$ with the velocity $V_0 = 7.8km/s$, the beginning acceleration is absent, the vehicle mass is constant. We assume that the Earth is a sphere, its swirling is absent and the gravity force does not depend on altitude [7]. The density distribution is the following function of the altitude $H(km)$

$$\rho = \rho_0 exp(-H/H_m); \quad H_m = 7.11km. \tag{1}$$

To formule the optimization problem, let us suppose that t_m is the total flight time of the vehicle moving along this high part of the trajectory. In this case, the total convective heat flux at the stagnation point of the 3D blunt body surface Q' along trajectory can be calculated using the following relation:

$$Q'(V, H, t_m) = \int_0^{t_m} q_w(H(t), V(t), R^*, k, k_{wi})dt. \tag{2}$$

Here $q_w(H(t), V(t), R^*, k, k_{wi})$ is the heat flux at the stagnation point of the space vehicle 3D blunt body surface, $V(t)$ is the flight velocity, $H(t)$ is the flight altitude, k is equal to the ratio of the body surface main curvatures at the stagnation point, R^* is the character linear size of the problem, k_{wi} are the known parameters of the heterogeneous chemical reactions occuring at the body surface.

Let us consider the following variational problem: find the smooth functions $V(t)$ and $H(t)$ $(0 \leq t \leq t_m)$ which have the following two properties:

1. The value Q' is minimum;
2. The equilibrium temperature of the body surface at the stagnation point $T_w(t)$ does not exceed the preassigned limit value T_w^{max}.

This problem is solved with the following constraints:

$$V(0) = V_0, \quad H(0) = H_0; \qquad V(t_m) = V^*, \quad H(t_m) = H^* \tag{3}$$

$$|\dot{V}(t)| < ag, \qquad |\dot{V}| \leq \frac{S^*}{m}\frac{\rho_\infty(t)V^2(t)}{2} \tag{4}$$

Here S^* is a reference area charaterising the body surface, m is the mass of the vehicle.

The relations in (3) mean that the trajectory begins from the point (V_0, H_0) and finishes at the point (V^*, H^*). The first relation in (4) is connected with the medical restrictions to the flight conditions. The second condition (4) [7] is rather obvious from physical point of view and in fact it means, that the deceleration along trajectory cannot exceed the maximum drag deceleration depending from a maximum drag force for the given body, for the given altitude and for the given flight velocity.

As initial mathematical model for calculating the integral in (2) we will use the thin (hypersonic) viscous shock layer equations. These equations are the asymptotic form of the Navier-Stokes equations and permit us to correctly describe the flow structure between the body surface and the shock wave if the following conditions are realized:

$$\varepsilon = \frac{\gamma - 1}{\gamma + 1} \to 0, \;\; Re \to \infty, \;\; K = \varepsilon Re \geq O(1).$$

The analysis demonstrates that this model has a good accuracy for our range of V and H for all possible trajectories [4].

At the stagnation point this equations system in the Dorodnicin variables has the following form [5]:

$$(l(u^\alpha)')' + Du^\alpha = k_\alpha (u^\alpha)^2 + \frac{P_\alpha}{\rho}, \qquad \alpha = 1, 2, \tag{5}$$

$$\Big(\frac{lc_p}{Pr}\theta'\Big)' + c_p D\theta' = \sum_{k=1}^{N} \Big(c_{pk} X_k \theta' + h_k \frac{\dot{W}_k}{\rho}\Big), \tag{6}$$

$$X_i' - Dc_i' = \frac{\dot{W}_i}{\rho}, \quad i = 1, 2, ..., N-1, \quad D = (k_1 f_1 + k_2 f_2)\frac{d}{d\eta}, \tag{7}$$

$$p = \rho\theta \frac{R_A T_0}{V_\infty^2}, \qquad P_\alpha' = 2\Delta k_\alpha^2 (u^\alpha)^2 \tag{8}$$

$$X_i = \alpha_i c_i' + \beta_i c_i, \qquad i = 1, 2, ..., N-1, \tag{9}$$

Here

$$\xi^\alpha = x^\alpha, \qquad \eta = \frac{1}{\Delta}\int\limits_0^{x^3} \rho dx^3, \qquad \Delta = \int\limits_0^{x_s^3} \rho dx^3, \qquad u^\alpha = f'_\alpha,$$

$$X_i = \frac{I_i}{\Delta}, \qquad l = \frac{\mu\rho}{Re\Delta^2}, \qquad P_\alpha = \frac{1}{k_\alpha \xi^\alpha}\frac{\partial p}{\partial \xi^\alpha}, \qquad A' \equiv \frac{\partial A}{\partial \eta},$$

$$\alpha_i = -\frac{l b_{(ii)}}{S m_{lN} a_{(ii)}}, \qquad \beta_i = a_{ii}^{-1} \sum_{j=1, j\neq i}^{N-1} (a^*_{ij} X_j + c'_{j\eta}\frac{l b^*_j}{S m_{lN}}),$$

$$a_{ij} = -a^*_{ij} c_i, \quad b_{ij} = -b^*_j c_i, \quad (i \neq j), \qquad a^*_{ij} = \frac{m_N S_{ij}}{m_j S_{lN}} - \frac{S_{iN}}{S_{lN}},$$

$$b^*_j = \frac{m_N}{m_j} - 1, \qquad a_{ii} = \frac{S m_{iN}}{S m_{lN}} + \sum_{j=1, j\neq i}^{N-1} a^*_{ij} c_j, \qquad b_{ii} = 1 + \sum_{j=1, j\neq i}^{N-1} b^*_j c_j.$$

Here the coordinate $R^* x^3$ is taken along the normal to the body surface; $R^* x^\alpha$ are the coordinates selected along the main direction on the body surface at the stagnation point, $R_\alpha = R^*/k_\alpha$ are the main radii of the body surface, $V_\infty u^*_\alpha u^\alpha$ $(\alpha = 1, 2)$, $V_\infty u^3$ are physical components of the vector velocity along x^α and x^3 directions. $V^2_\infty \rho_\infty P$, $\rho_\infty \rho$, $T_\circ \theta$, are respectively pressure, density, temperature of gas mixture, which consists of N components. $\mu(T_\circ)\mu$, $V_\infty c_p/(2T_\circ)$, $Pr = \mu c_p/\lambda$, $Re = \rho_\infty V_\infty R^*/\mu(T_\circ)$, m are viscosity, specific heat at constant pressure, Prandtl number, Reynolds number, molecular weight of the mixture respectively. c_i, m_i, $V^2_\infty h_i/2$, $V^2_\infty c_{pi}/(2T_\circ)$, $V_\infty \rho_\infty I_i$, $V_\infty \rho_\infty \dot{W}_i/R^*$, S_{ij} are mass concentration, molecular weight, specific enthalpy, specific heat, normal component of a diffusion flux vector, a formation velocity of $i-$ th species and binary Shmidt number.

The boundary conditions for the system of equations (5)-(9) are the following.

At the shock wave ($\eta = 1$) the hypersonic approximation of generalized Rankine - Hugoniot conditions are used:

$$l\Delta(u^\alpha)' + u^\alpha = 1, \quad (\alpha = 1, 2), \qquad \Delta(k_1 f_1 + k_2 f_2) = 1, \tag{10}$$

$$\frac{l c_p \Delta}{Pr}\theta' + \sum_{j=1}^{N} c_{j\infty}(h_j - h_{j\infty}) = 1, \qquad p = 1, \qquad P_\alpha = -2k_\alpha,$$

$$\Delta X_i + c_{i\infty} - c_i = 0, \qquad (i = 1, 2, ..., N-1)$$

At the body surface ($\eta = 0$) heterogeneous chemical reactions are taken into account and heat discharge inward of body is neglected:

$$u^\alpha = 0, \quad X_i = \dot{r}_i \Delta^{-1}, \quad i = 1, ..., N-1 \quad X_q = -\frac{G\theta^4}{\Delta} \quad , \tag{11}$$

Here

$$X_q = -\frac{lc_p}{Pr}\theta' + \sum_{j=1}^{N} h_j X_j, \quad G = \frac{2\varepsilon_I \sigma^* T_0^4}{\rho_\infty V_\infty^3}.$$

In this case, the value $q_w(H(t), V(t), R^*, k, k_{wi})$ can be calculated in the following way:

$$q_w(H(t), V(t), R^*, k, k_{wi}) = 0.5\rho_\infty V_\infty^3 X_q(H(t), V(t), R^*, k, k_{wi}) \tag{12}$$

The X_q value is calculated after solution of the boundary value problem (5)-(11).

Finally let us note that for boundary conditions (11) the integral

$$Q(V, H, t_m) = \frac{1}{t_m T_w^{max}} \int_0^{t_m} q_w^\circ(H(t), V(t), R^*, k, k_{wi}) dt. \tag{13}$$

and the integral Q' (see (2)) achieve their minimums simulltaneously (for the same trajectory).

3 SOLUTION METHOD

For solution of the above optimization problem a variant of the floating-point Genetic Algorithms is used. Floating-point Genetic Algorithms realise a compromise between binary-coded Genetic Algorithms and Evolution Strategies [8], since they use most of the classical Genetic Algorithms mechanisms whereas they work directly at the phenotypic level like Evolution Strategies.

We used ordinary single point, uniform or arithmetical crossover operator. Let us suppose that individuals $A = (a_1, ..., a_i, a_{i+1}, ..., a_n)$ and $B =$

$(b_1, ..., b_i, b_{i+1}, ..., b_n)$ are chosen from selection process as parents. The ordinary single point crossover operator produce the following two children $A' = (a_1, ..., a_i, b_{i+1}, ..., b_n)$ and $B' = (b_1, ..., b_i, a_{i+1}, ..., a_n)$ (where i is a random cutten point).

If r_i is a random number in the interval $[0; 1]$ the uniform crossover operator produces the following two children $A' = (a'_1, ..., a'_i, ..., a_n)'$ and $B' = (b'_1, ..., b'_i, ..., b'_n)$ where

$$a'_i = \begin{cases} a_i & r_i \leq 0.5 \\ b_i & r_i > 0.5 \end{cases} \qquad b'_i = \begin{cases} a_i & r_i > 0.5 \\ b_i & r_i \leq 0.5 \end{cases}$$

For the arithmetical crossover operator the values a'_i and b'_i are calculated using the following formula

$$a'_i = (1 - a)a_i + ab_i, \qquad b'_i = (1 - a)b_i + aa_i$$

where $a = -0.5 + 1.5r$, and r is a random number in the interval $[0; 1]$.

As the mutation operator, we use the nonuniform mutation operator defined by Michalewicz [9]. If a gene y_i is to mutate, the new value y'_i is chosen at random within interval $[Min_i, Max_i]$ by the following formula:

$$y'_i = y_i + s(M_i - y_i)\Big(1 - \frac{g}{G}\Big)^b \tag{14}$$

s is a random number from $[0, 1]$, g is the generation number, G is the maximal generation number, b is the refinement parameter, M_i is randomly chosen from Min_i and Max_i (lower and upper bounds of the variable y_i).

One of the main problems that arises in GAs is premature convergence. For solution of this problem we used the Distance-Dependent Mutation approach [10]. This approach consists in using the distance between the two mates in order to compute the mutation rate: the mutation rate is no longer a constant parameter, it is dynamically computed for both children and depends on the parents. Every time a couple of individuals is chosen for mating, the mutation rate is computed and will be applied to their children after crossover occurs. If the parents are quite close (i.e. their mating is likely to be considered as incest), that would lead to a high mutation rate for their children, whereas mutation rate will be smaller if they are distant. As a distant criteria we took

a relative distance that takes into account the bounds of each variable of the individual. If $A = (a_1, ..., a_i, ..., a_n)$ and $B = (b_1, ..., b_i, ..., b_n)$ be the two mates

$$dist(A, B) = \frac{1}{n} \sum_{i=1}^{n} \left(\frac{a_i - b_i}{Max_i - Min_i} \right)^d$$

d is a distance parameter that can be used to adjust the way the distance is computed.

Let $M_r(A, B)$ be the mutation rate ($M_r(A, B) = 1 - dist(A, B)$). If A and B are identical, we have $M_r(A, A) = 1$ which means that there will be a compulsory mutation on each variable of the children. That is clearly a too strong mutation, and in order to avoid that, we introduce M_m which corresponds to the maximum mutation rate that is allowed.

$$M_r(A, B) = M_m(1 - dist(A, B))$$

In our calculations we took $d = 0.2$.

So, our optimization method involved the following pseudo code:
$t := 0$
initpopulation $P(t)$ */* random or random + initial solution(s) */*
while not done do

- $P' :=$ selectparents $P(t)$
  / tournament selection */*
- recombine $P'(t)$
  / single point, uniform or arithmetical crossover */*
- mutate $P'(t)$
  / nonuniform + distance-dependent mutation */*
- evaluate $P'(t)$
- $P(t+1) := P'(t) \oplus \text{best}(P)$
  / elitism */*
- $t := t + 1$

enddo

For approximation of the trajectory we used Bezier Spline representation. As it is known a Bezier curve of order N is defined by the Bernstein polynomials $B_{N,i}$ (C_N^i - binomial coefficients)

$$\vec{G}(s) = \sum_{i=0}^{N} B_{N,i}\vec{P}_i, \quad B_{N,i} = C_N^i s^i (1-s)^{N-i}, \quad C_N^i = \frac{N!}{i!(N-i)!}, \tag{15}$$

where s denotes the parameter of the curve taking values in $[0,1]$, $\vec{P}_i$ are the control points. So, as it is seen from (15) the Bezier curve is completely determined by the cartesian coordinates of the control points.

For our optimization problem, the parameter s is equal to the dimensionless time $\tau = t/t_m$ and Bezier approximation of the trajectory is determined by coordinates $(\bar{H}_i, \bar{V}_i)$ of the control points $\vec{P}_i$ where

$$\bar{H} = \frac{H - H_0}{H^* - H_0}, \quad \bar{V} = \frac{V - V_0}{V^* - V_0}$$

The first $\vec{P}_0 = (0,0)$ and the last $\vec{P}_m = (1,1)$ points are fixed, which corresponds to conditions (3). This means that our string S=$(a_1, a_2, ..., a_{N-1}, a_N, ..., a_{2N-2})$ has the following form:

$$S = \begin{cases} a_i = \bar{H}_i, & 1 \le i \le (N-1) \\ a_i = \bar{V}_{i-N+1}, & N \le i \le (2N-2) \end{cases}$$

So, a string S contains $2N-2$ values of control points. These values are varied from Min_i to Max_i which are lower and upper bounds of the variable a_i.

Because the constraints for the optimization problem are inequalities during realization of these algorithms we modified the objective function. In our case we used the following modified objective function Q^*:

$$Q^* = \begin{cases} q_1 + q_2(|\dot{V}(t)|/g - a), & \text{if } |\dot{V}(t)| > ag, \\ q_3 + q_4(T_w^{\max} - T_w)/T_w^{\max}, & \text{if } T_w > T_w^{\max}, \\ q_5 + q_6(|\dot{V}(t)|/g - A(t)/g) & \text{if } |\dot{V}(t)| > A(t), \\ Q, & \text{in other cases} \end{cases} \tag{16}$$

where $A(t) = S^*\rho(t)V^2(t)/(2m)$ and q_i are the problem depended parameters.

In fact, this approach enables one to extend the search space and to evaluate in terms fitness the individuals, that do not satisfy to the constraints of the optimization problem. It is very important to note that differing from conjugate gradient optimization methods GA methods are not any restrictions on a smoothness of this extension.

4 RESULTS AND DISCUSSIONS

The solution of this variational problem was obtained for the following range of problem and GA parameters:

$$\frac{S^*}{m} = 2.5 \cdot 10^{-3}\mathrm{m}^2/\mathrm{kg}; \qquad a = 3.0;$$

$$T_w^{max} = 1500K, 2500K; \quad k = 0.4, 1.0; \quad R^* = 0.5m, 1.0m.$$

$$V_0 = 7.8\mathrm{km/s}, \quad V^* = 2.3\mathrm{km/s}, \quad H_0 = 100\mathrm{km}, \quad H^* = 50\mathrm{km},$$

$$0.4 \leq P_c \leq 1.0; \quad 0.1 \leq M_m \geq 0.9; \quad S = 20, 50, 100, 200;$$

$$B = 10, 20; \quad G = 2000,\ 5000,\ 10000; \quad 8 \leq N \leq 13$$

where P_c is a crossover probability, M_m is a maximum allowed mutation probability, S is a population size.

It is understood that the calculation of the integral (13) via the direct numerical solution of the TVSL equations system at each trajectory point requires a very large computer resource. For this reason, we have used the following approximate approach. At the first step the initial boundary value problem (5)-(11) was solved for given values R^*, k, k_{wi} on grid 21×22 with step $\Delta V_\infty = 0.25km/s$ (for velocity range from 7.8 km/s to 2.3 km/s) and with step $\Delta H = 2.5km$ (for altitude range from 100 km to 50 km). At the second step we calculated the objective function (13) via interpolation of the obtained results on the velocity an on the altitude using B-spline representation.

The comparisons demonstrated that the difference between integral heat flux along different trajectories, calculated on the basis exact and the above listed two-step approximate approach did not exceed $0,5\%$, which permits us to use this method for serial calculations.

Together with the initial problem solution we considered the solution of the following inverse problem: find the reentry trajectory with given distribution of the heat flux at the stagnation point of the 3D blunt body along trajectory. In this case for the given trajectory on the base of the TVSL equations solution the distribution of the heat flux along the given trajectory was determined. After that, the minimization problem of the following cost function was solved:

$$q_r = \frac{1}{M q_w^*(0)} \sqrt{\sum_{i=1}^{M} \left[q_w(t_i) - q_w^*(t_i) \right]^2} \tag{17}$$

where M is the grid number along coordinate t, $q_w^*(t_i)$ is the known value of a heat flux to a body surface in a time point $t = t_i$.

The solution of this inverse problem is very important from methodical point of view. If we assume the correspondence between the reentry trajectory and the distribution of the heat flux along it (for other fixed parameters of a problem) is one-to-one, the solution of this problem of optimization is known: a minimum value q_r is equal to zero and the reentry trajectory obtained from solution of our optimization problem should coincide with the given one. In addition, because in this case we know the solution of the problem we have a good way to verify the algorithm accuracy and to estimate its robustness and its efficiency.

One example of this inverse problem solution is presented in fig. 1, where the distributions V/V_0 and H/H_0 versus time τ (fig. 1a) and H versus V (fig. 1b) are drawn. Here lines a - given trajectory, lines b - the solution of the inverse problem.

Let us stop in the beginning on some outcomes of a numerical solution of an inverse problem. The results of the systematic calculations demonstrated that the suggested algorithm is quite robust, has a good accuracy and a high level of arithmetical cost efficiency: for $S = 50$, $N = 10$ the value of q_r for 80% of runs does not exceed 10^{-6} after 1000 generations (the obtained trajectory with a graphic accuracy coincided with the given one) and the CPU time for one variant was equal to 3-5 min (on a computer SUN US1/143).

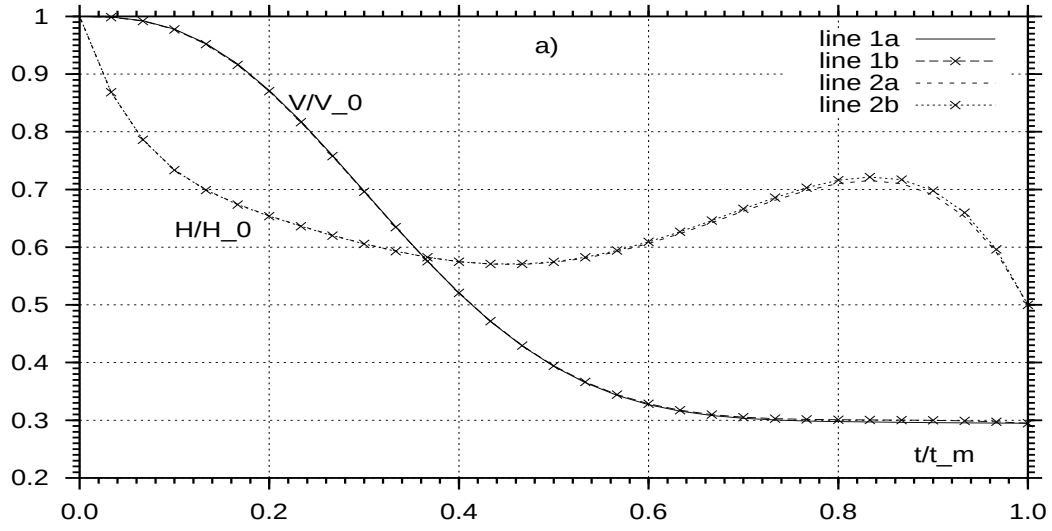

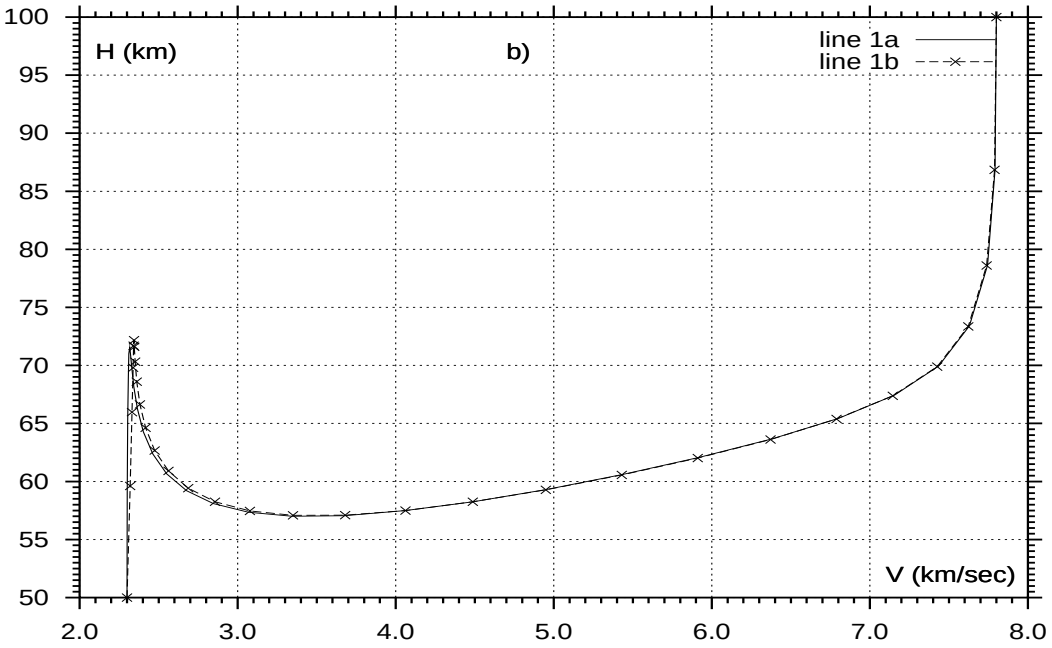

Figure 1: Solutions of the inverse problem (lines b). $S = 50$, $N = 10$, $q_r = 3.43 \cdot 10^{-7}$, $t_m = 30min$. Lines a : given trajectory.

4.1 The influence of the GA parameters.

First of all we investigated the influence of the GA parameters on the solution accuracy and on the algorithm efficiency. All these investigations were carried out for noncatalytic body surface and for the following values of the problem parameters:

$$\frac{S^*}{m} = 2.5 \cdot 10^{-3}\mathrm{m}^2/\mathrm{kg}; \quad a = 3.0; \quad t_m = 30min;$$

$$T_w^{max} = 1500K; \quad k = 1.0; \quad R^* = 1.0m.$$

At the begining the dependence of the optimal solution from the order N of the Bezier spline was studied. Some results of this investigation are presented in Tabl. 1, where you can see the best five values of the objective function Q (from 20 runs) for different N.

Table 1

$N = 8$	$N = 9$	$N = 10$	$N = 12$	$N = 13$
1.5285	1.1316	1.1224	1.1212	1.1211
1.5313	1.1361	1.1235	1.1221	1.1219
1.5379	1.1362	1.1239	1.1228	1.1232
1.5387	1.1381	1.1247	1.1233	1.1234
1.5416	1.1385	1.1284	1.1251	1.1247

It was established that the minimal sufficient value of parameter N is equal to 10. Methodical calculations have shown, that since a parameter $N = 10$ further increasing of N value did not produce an improvement of an obtained solution - appropriate trajectories coincided with a graphic exactitude. Thus, hereinafter all basic calculations were carried out at $N = 10$.

It is necessary to note, that using elitist mechanisms and mutation probability dependence on a distance between the parents really improves the convergence and the accuracy. Therefore both these mechanisms have always been used in all calculations.

Another very important parameter for GA algorithms is the population size S. As it is known from the theory, increasing this value, result in a diminution of the number of iterations, which are necessary for convergence, but does not

result in an essential diminution of expended CPU time. It means that for higher algorithm efficiency we have to decrease the population size with saving appropriate solution accuracy. It is also rather obvious that the influence of the parameter S on the GA algorithm properties is rather strongly connected with a allowed variation range of genes.

Thus for this investigation we used the following two-stage approach. Because at the beginning no information about appropriate variation range of Min_i and Max_i at the first stage is known we started our calculations with rather high value of the population size S and with maximum possible variation of lower and of upper bounds of the variables $\bar{H}_i$ and $\bar{V}_i$ (for fixed generations number g_m).

For our case, we did 10 runs with the following values of these parameters:

$$S = 100 - 200; \quad g_m = 1000 \quad Min_i = 0; \quad Max_i = 1.0; \quad (i = 1, ..., 2N - 2)$$

At the end of the first stage we calculated the average value of variables a_i^{av} for best individuals from best five runs. After that, we determined the new values of Min_i and Max_i in the following way:

$$Min_i = 0.75 a_i^{av}; \quad Max_i = 1.25 a_i^{av}$$

These new values of Min_i and Max_i were a starting point for the second stage of our problem solution where for serial calculations we used rather low population size value.

The systematic calculation indicated that suggested approach essentially improved the algorithm efficiency and permited one to obtain solutions with good accuracy using relatively low population size. As it can see from fig. 2-3, where we compare results of calculations for different S (lines a, b, c, d correspond to $S = 20, 50, 100, 200$), the algorithm covergence is rather high, the differernce of solution for $S = 20$ and $S = 200$ does not exceed 0.5% and trajectories and T_w distributions practically coincide.

Also we investigated the influence of the maximum mutation probability M_m on an accuracy and on a algorithm convergence for various mechanisms of a crossover and for various crossover probability values P_c. Some results of these computations are shown in fig.4 (for $P_c = 0.9$) and in fig.5 (for $P_c = 0.7$). Here the dependence of Q on the number of generation g (for the best individual in

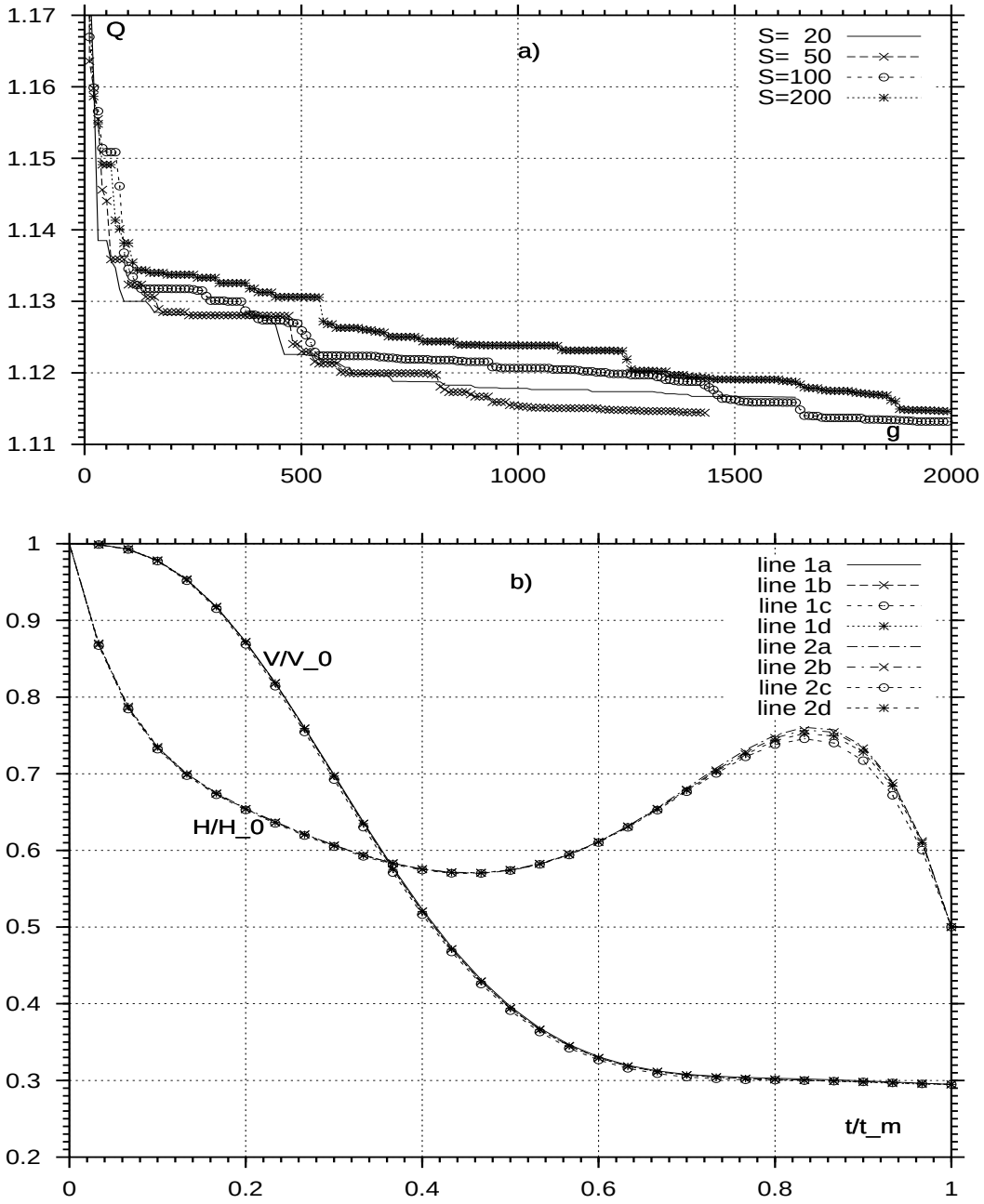

Figure 2: Distributions of the objective function Q versus generation number g (a), velocity V/V_0 and altitude H/H_0 (b) along trajectory for different population sizes. Lines a, b, c, d : $S = 20, 50, 100, 200$.

b)

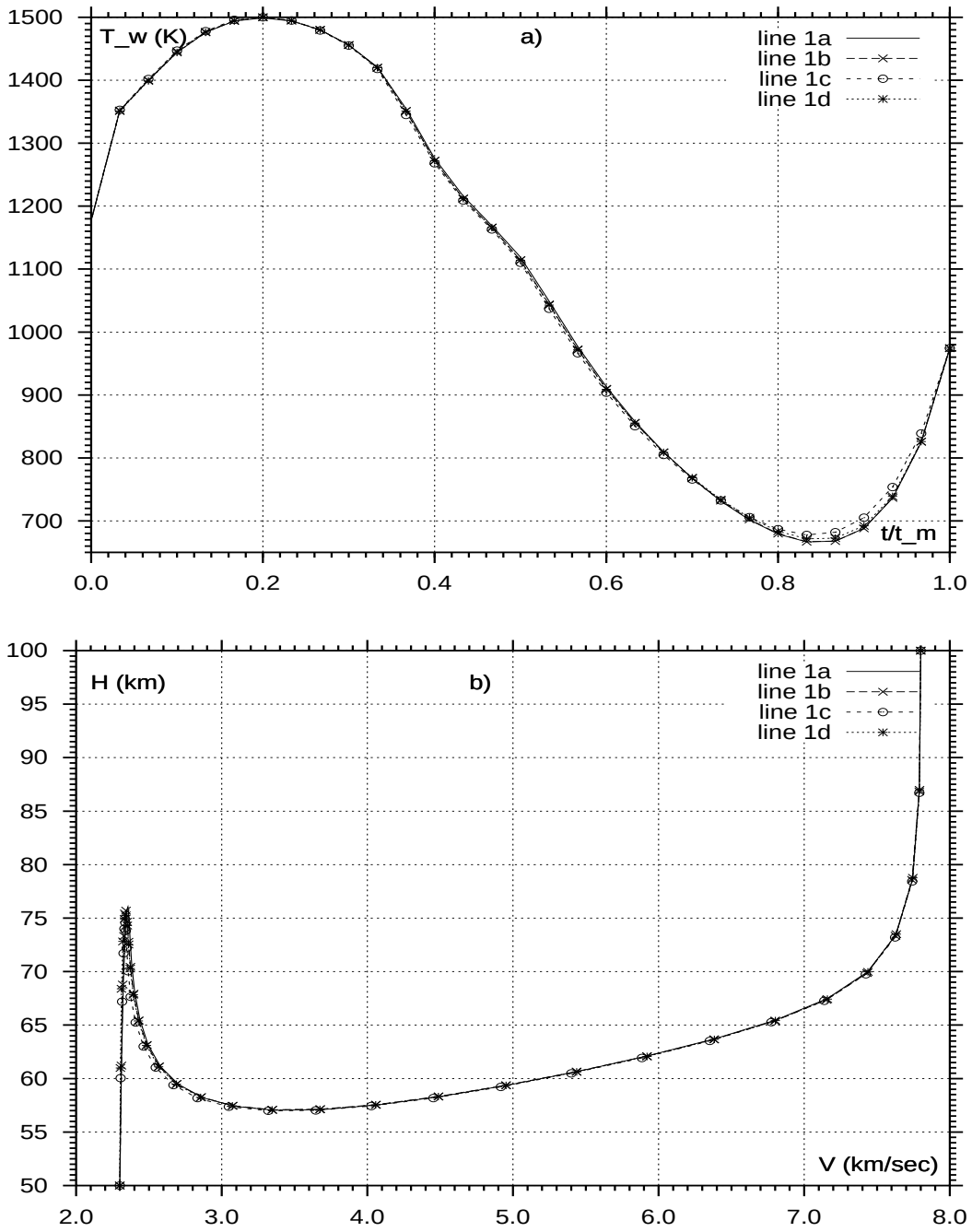

Figure 3: Distributions of T_w along trajectory (a) and altitude H versus velocity V (b) for different population sizes. Lines a, b, c, d : $S = 20, 50, 100, 200$.

a population) in the "best" calculation (minimum value for 10 runs) for single-point crossover (fig.4a, fig.5a) and for arithmetical crossover (fig.4b, fig.5b) are presented. As it can see, from these pictures the best results for all crossover types are obtained for relativly low level of the maximum mutation probability $M_m = 0.05 - 0.1$.

As for influence of the crossover type the analysis of the obtained results allows one to conclude, that the worst results are given by uniform crossover. The arithmetical crossover gives slightly improved results in comparison with single-point at the expense of a possibility of the appearance of a positive information both in a result of a mutation and in a result of a crossover.

The crossover probability was also varied between reasonable limits (from 0.4 to 1.0) and as a result it was established that the optimum value is $P_c = 0.9$. The parameters G and b, adequate for a velocity of a rescaling of a mutation were varied in the following range: $2000 \leq G \leq 20000$, $5 \leq b \leq 20$. The character of these parameters influence on an algorithm convergence can be seen from fig.6 where dependence Q on the number g of generations for the best individual in a population in the "best" calculation (minimum value for 10 runs) for for arithmetical crossover, for $M_m = 0.05$ and for various G and b are presented.

The numerical experiments have shown, that the best results are obtained with $G = 10000$, $b = 10$. If we increase parameter G up to 20000 it leads to unjustified deceleration of a convergence, and in turn its diminution up to 2000 leads to premature convergence and a deterioration of the obtained results accuracy.

As a whole taking into account the results of these systematic calculations all further computations were carried out for an arithmetical crossover and for the following values of GA parameters

$$P_c = 0.9, \quad M_m = 0.1, \quad G = 10000, \quad b = 10$$

4.2 The influence of the problem parameters on the optimal trajectory.

First of all let us consider the influence of the total flight time t_m on the optimum trajectory. Some results of these investigations are presented in fig.7-8,

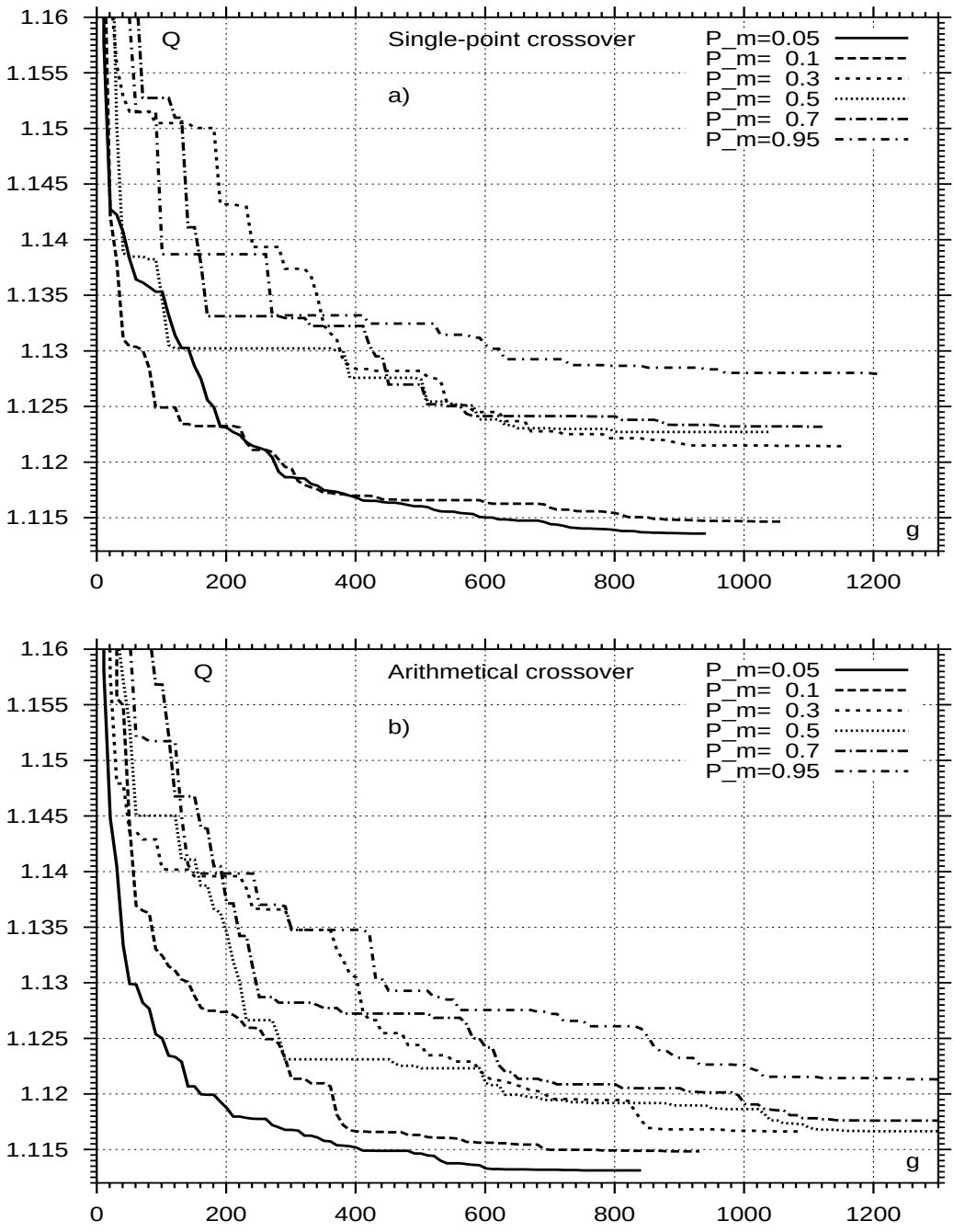

Figure 4: Distributions of the objective function Q versus generation number g for different mutation probability values and for $P_c = 0.9$, $S = 50$.

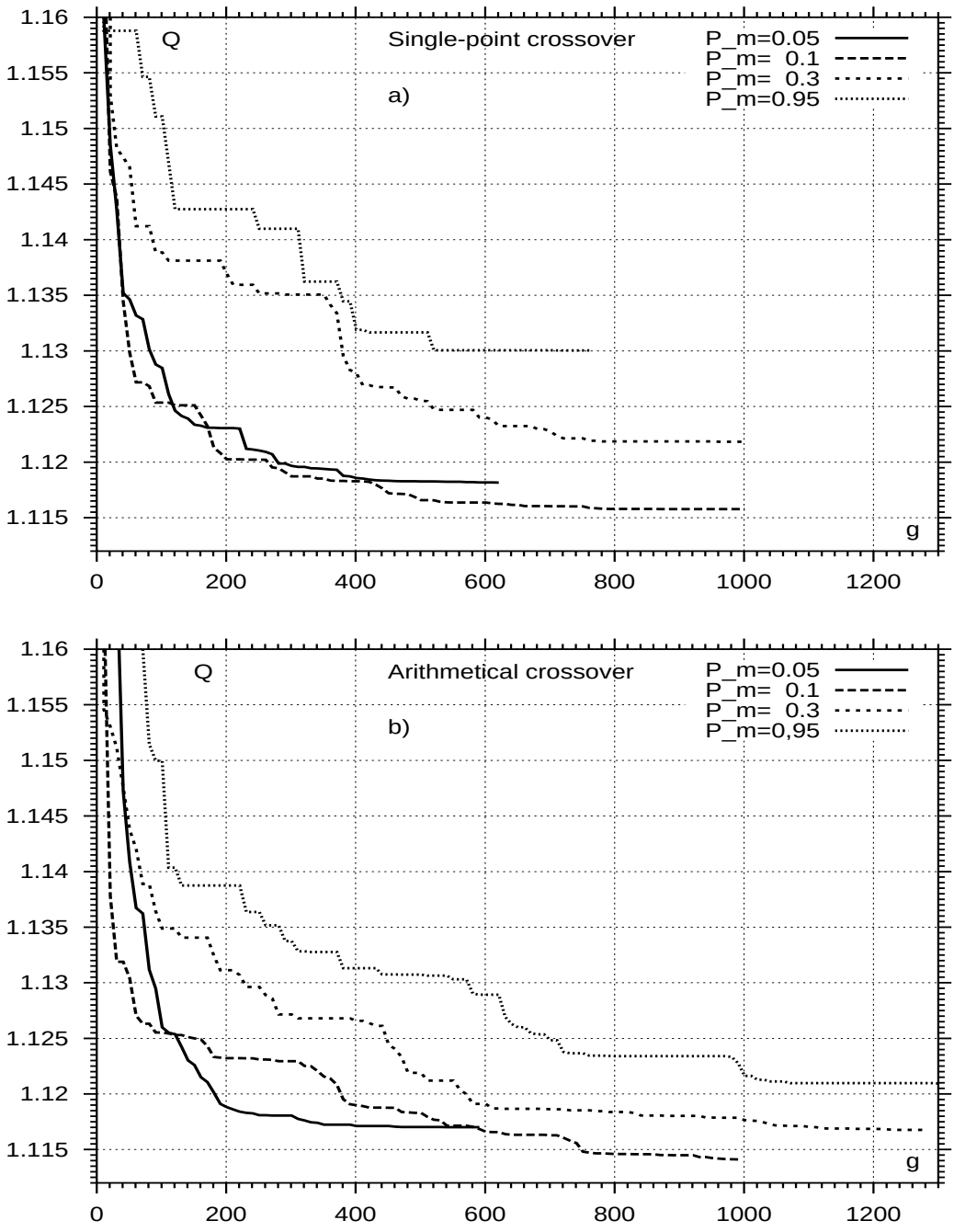

Figure 5: Distributions of the objective function Q versus generation number g for different mutation probability values and for $P_c = 0.7$, $S = 50$.

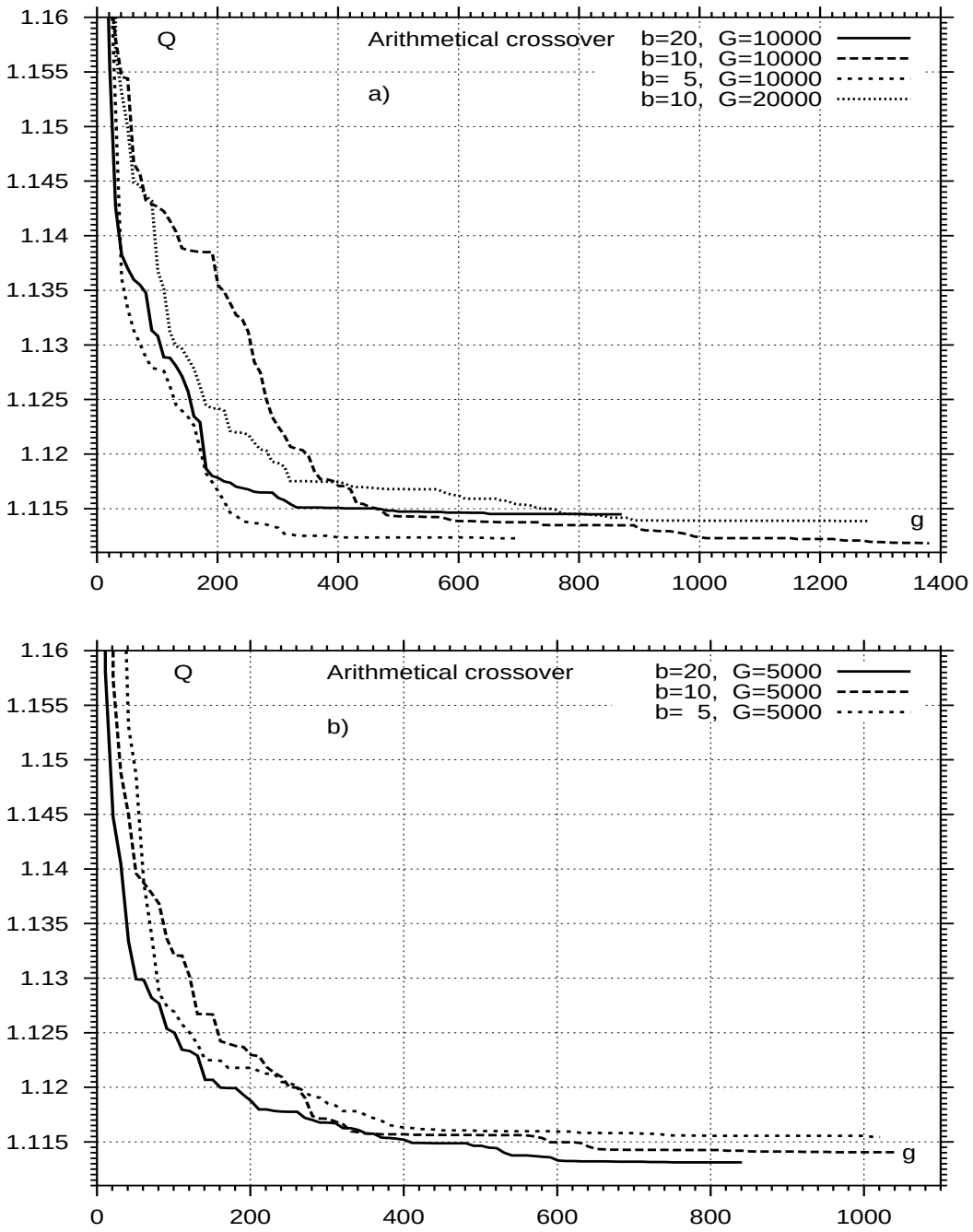

Figure 6: Distributions of the objective function Q versus generation number g for $S = 50$, for various values for the maximum allowed generation render G and various values for the parameter b.

where the distributions of temperature T_w versus τ (fig.7a), of altitude H versus velocity V (fig.7b), of accelaration dV/dt along trajectory (fig.8a), of altitude H/H_0 and of velocity V/V_0 versus time τ (fig.8b) for different total flight time t_m are shown. Lines a, b, c in fig.8 correspond to $t_m = 30min, 20min, 15min$, lines 1,2 in fig.8a correspond to maximum allowed drag acceleration along these trajectories and acceleration values realized along optimum trajectories.

As it can be seen from fig.7a the distributions of $T_w(\tau)$ along optimum trajectories have two segments. At the first one the equilibrium body surface temperature T_w reaches the maximum allowed value and has a local 'plateau'. At the second segment this value has a minimum. The length of this "plateau", the position and the value of this minimum depends on the total flight time t_m: if for $t_m = 30min$ the "plateau" length is equal to 5% of the total flight time and T_w has a local minimum at $\tau = 0.82$ then for $t_m = 15min$ the "plateau" length is increased to 30% of the total flight time and the minimum of T_w is reached ar the end trajectory point.

It is necessary to note that this character of the heat flux distributions along optimal trajectories is rather clear from physical point of view. Because the heat flux to the body surface is decreased if a flight velocity V is decreased and (or) a flihgt altitude H is increased and taking into account boundary conditions for V and H the possible optimum strategy is to reach a lower velocity level at a higher altitude and then to move with smaller velocity.

In fact this strategy is realized in our optimum solution: taking into account the constraints on T_w and on a vehicle acceleration (depending from the aerodynamic characteristics of the space vehicle) at the first segment of trajectory the decrease of the velocity at the upper part of the trajectory is reached. The optimal strategy at the second flight segment depends on t_m. For long total flight time the altitude is not a monotonic decreasing function. Instead after first phase of flight the altitude is gained to reduce the heat flux and then again altitude decrease to match trajectory essentually target point. But for short t_m there is not enough time to realize an altitude non-monotonic part of trajectory and after first trajectory stage the altitude and the velocity are monotonically decreased to satisfy boundary conditions at the end point of trajectory.

It is very important to note from methodological point of view that as it is seen from fig.7a, 8a our physical constraints are very essential during most

of the trajectory. It means that the optimal point in our search domain is very close to the boundary of this domain and a application of the conjugate gradient optimization methods to the solution this optimization problem would imply a number of difficulties to calculate with high accuracy derivatives of the objective function near space search boundary.

Thus the optimum trajectory shape for the fixed value of the T_w^{max} depends on the aerodynamic characteristics of the space vehicle (ratio S^*/m) and on the total entry time t_m.

From the methodological point of view it is also interesting to investigate the dependence of the optimum solution on T_m^{max}. First of all, we considered the limit case, when this value is very high and it can not be reached at all appropriate trajectories. In fact, for the limit case the constraint on the maximum allowed value of T_w has no effect on the problem solution. The results of these calculations for $T_m^{max} = 2500K$ are presented in fig.9-10, where the distributions of temperature T_w versus τ (fig.9a), of altitude H versus velocity V (fig.9b), of accelaration dV/dt along trajectory (fig.10a), of altitude H/H_0 and of velocity V/V_0 versus time τ (fig.10b) for different total flight time t_m are shown. Lines a, b, c, d in fig.10 correspond to $t_m = 10min, 15min, 20min, 30min$, lines 1,2 in fig.10a correspond to maximum allowed drag acceleration along these trajectories and acceleration values realized along optimum trajectories. As it can be seen for this limit case for all considered reasonable total flight time t_m all optimum trajectories have a second flight segment with non-monotonic behaviour of the flight altitude.

But if we decrease the T_w^{max} value the optimal solution character changes (by similar way for different flight times): the value of the local maximum in H distributions decreases and for rather low T_w^{max} this maximum disappears. Some results of calculations for various T_w^{max} and for different total flight time ($t_m = 10min, 15min, 20min, 30min$) are shown in fig.11-14. The equilibrium body surface temperature distributions along optimal trajectories are also changed rather strongly: for rather low T_w^{max} a local minimum in T_w disappears, length of a "plateau" is increased and its value is reduced. As a whole these results demonstrate that the parameter T_w^{max} has very strong influence on solution of the optimization problem.

It is rather obvious from physical point of view, that because T_w strongly depends on R^* and k_{wi} the initial variational problem has no solution for

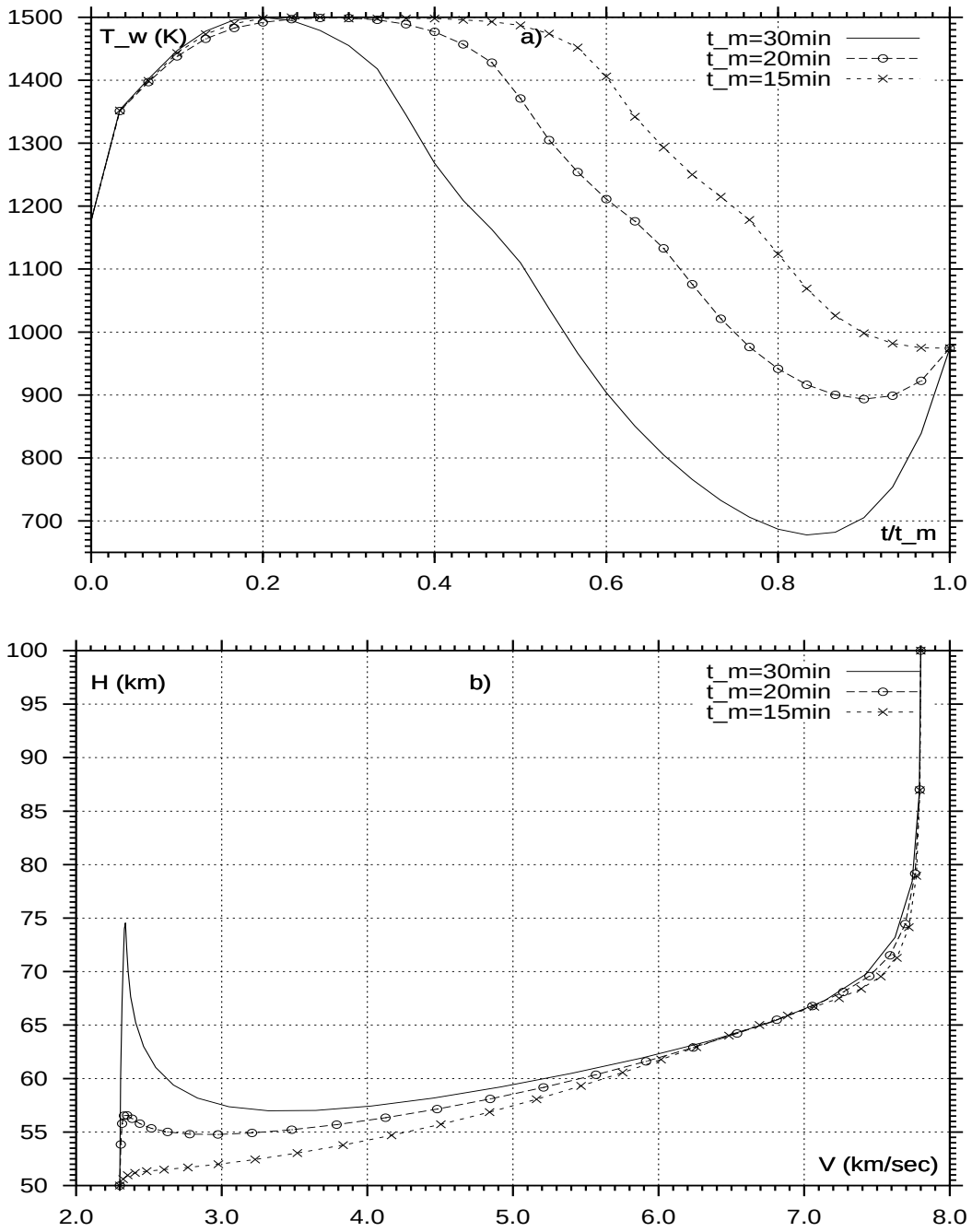

Figure 7: Distributions of temperature T_w versus τ (a) and altitude H versus velocity V (b) for $T_m^{max} = 1500K$ and for different total flight times t_m

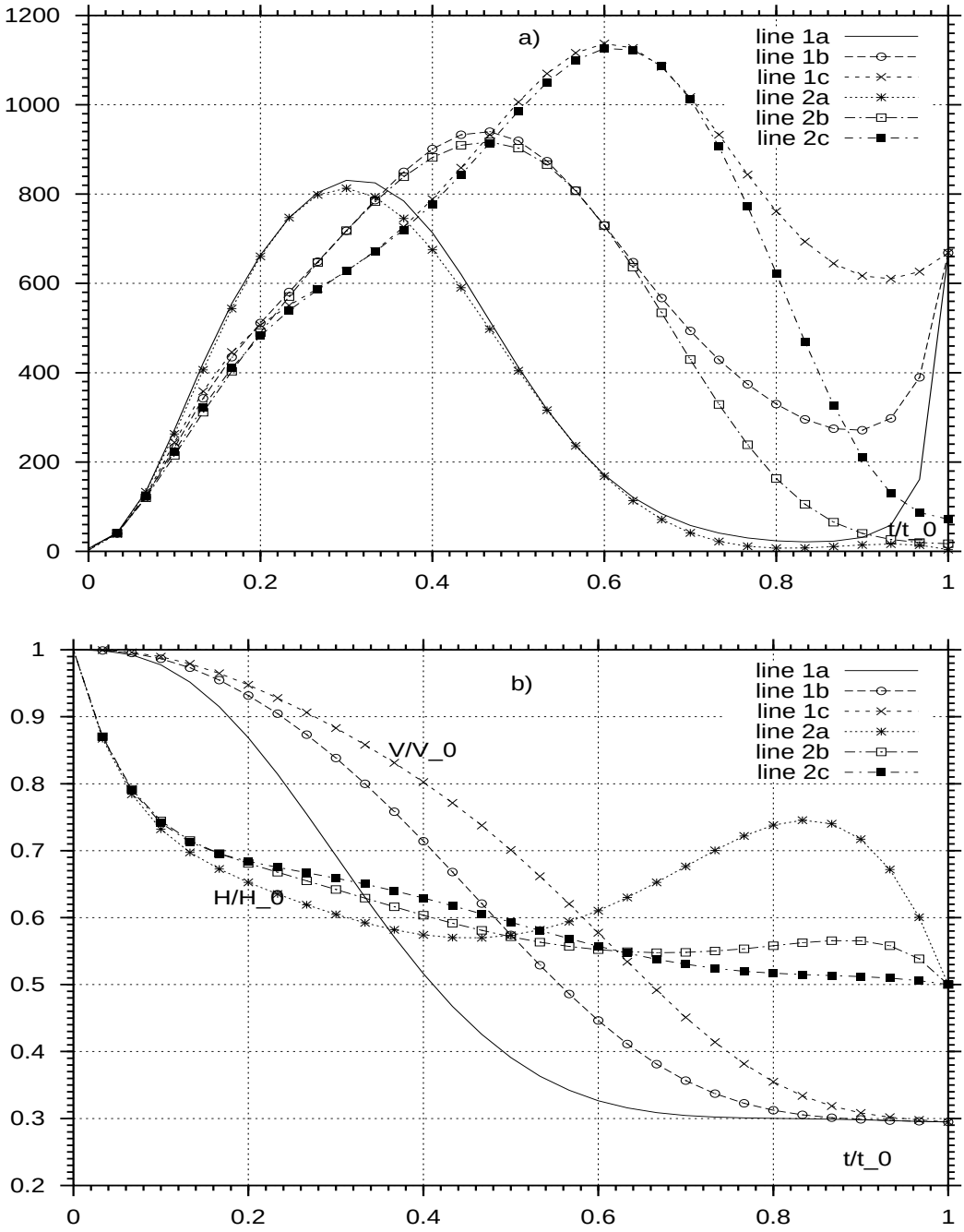

Figure 8: Distributions of deceleration dV/dt (sm/s^2) along trajectory (a), altitude H/H_0 and velocity V/V_0 versus time τ (b) for $T_m^{max} = 1500K$ and for different total flight times t_m. Lines a, b, c : $t_m = 30min, 20min, 15min$.

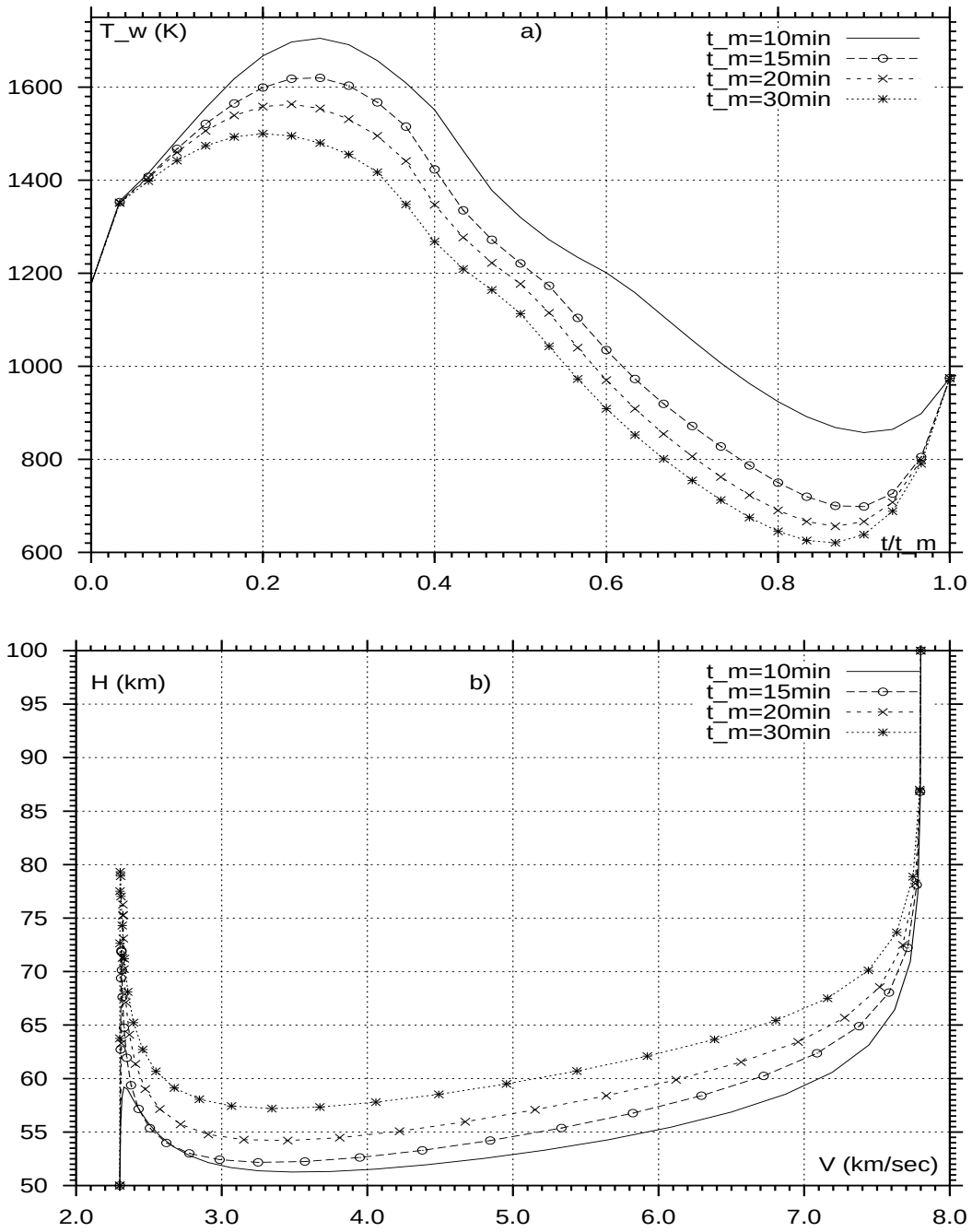

Figure 9: Distributions of temperature T_w versus τ (a) and altitude H versus velocity V (b) for $T_m^{max} = 2500K$ and for different total flight times t_m.

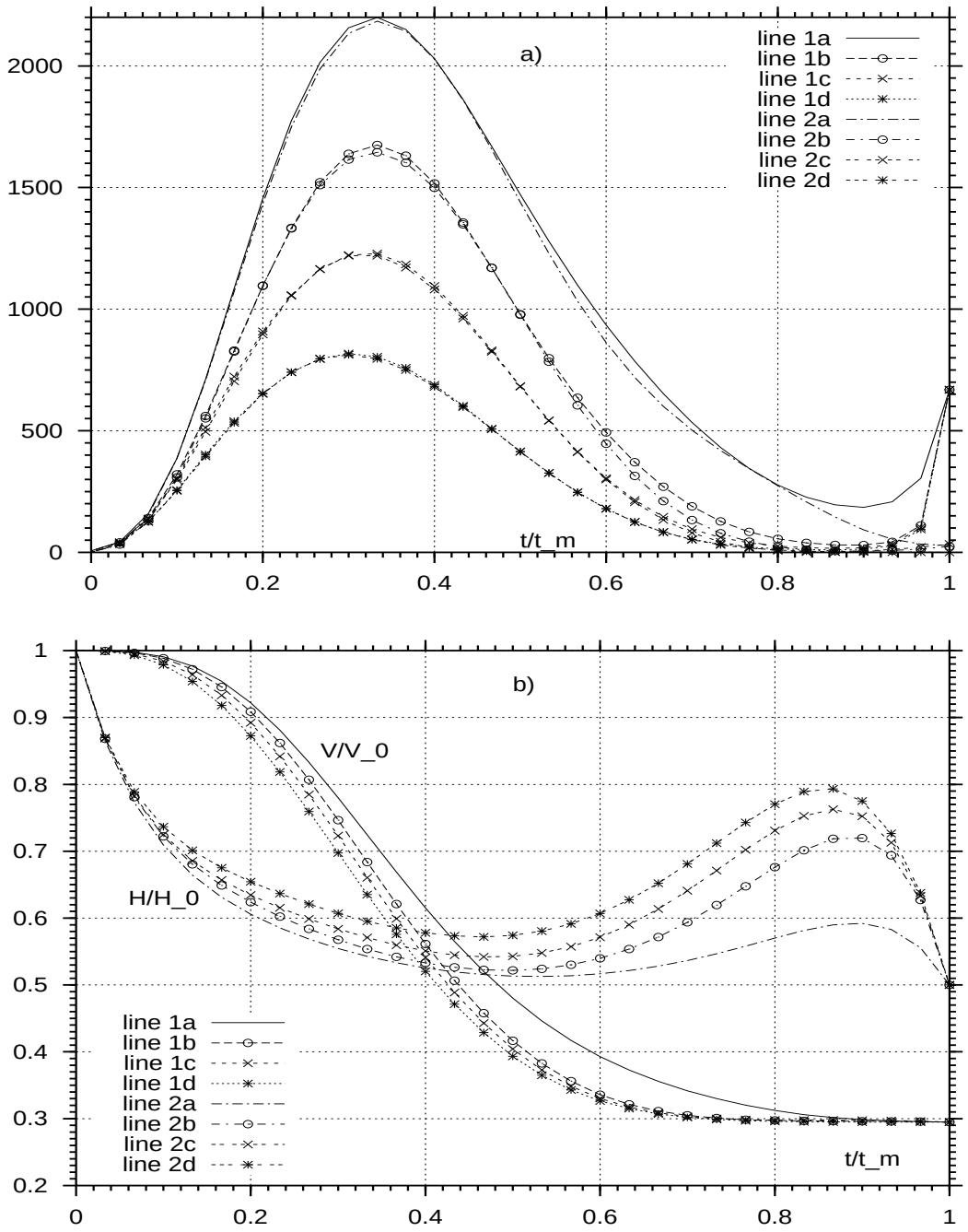

Figure 10: Distributions of deceleration dV/dt (sm/s^2) along trajectory (a),altitude H/H_0 and velocity V/V_0 versus time τ (b) for $T_m^{max} = 2500K$ and for different total flight times t_m. Lines a, b, c, d : $t_m = 10min, 15min, 20min, 30min$.

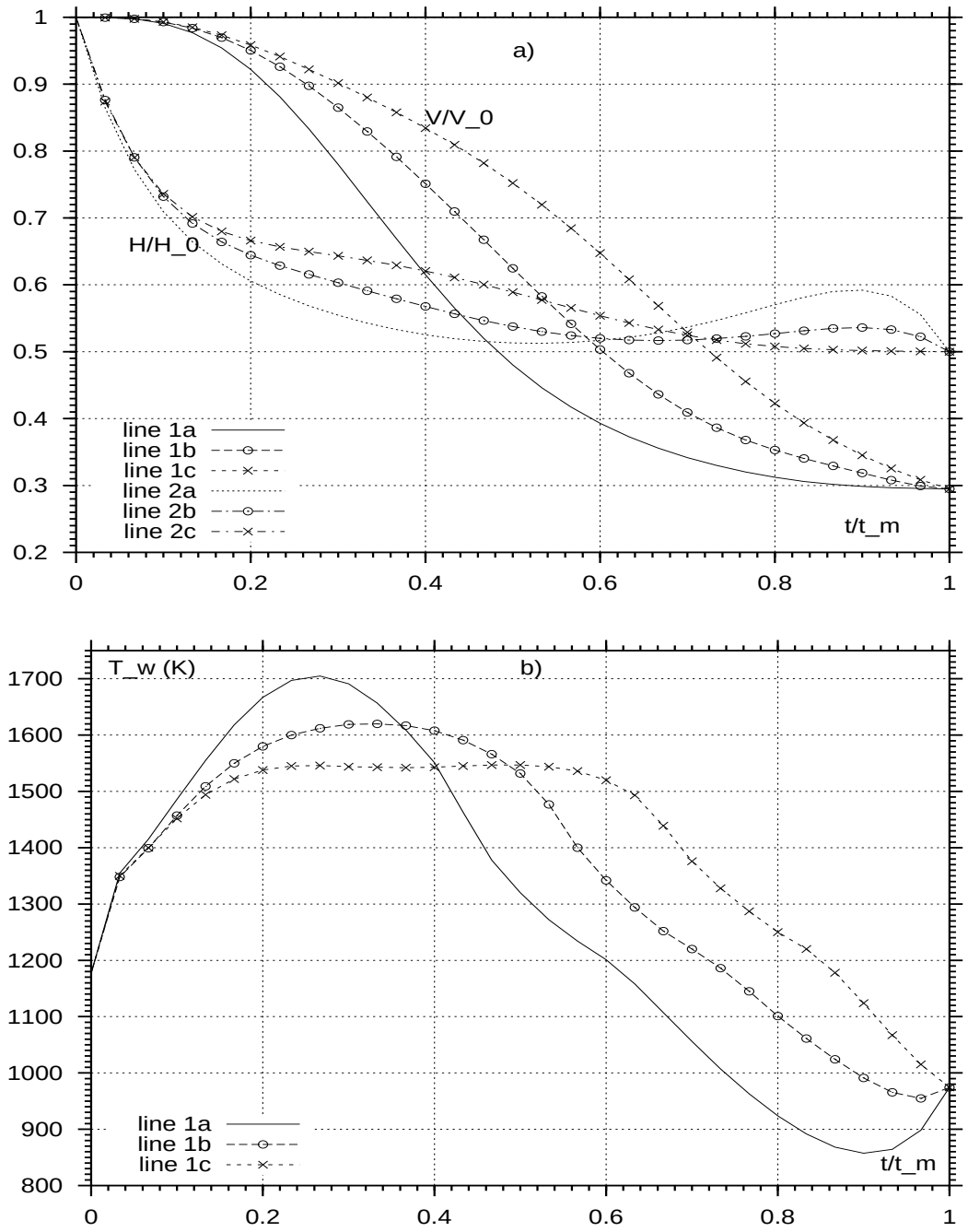

Figure 11: Distributions of temperature T_w versus τ (b), altitude H (lines 2) and velocity V (lines 1) versus τ (a) for various T_w^{max} and for $t_m = 10min$. $T_w^{max} = 2500K, 1620K, 1547K$ - lines a, b, c

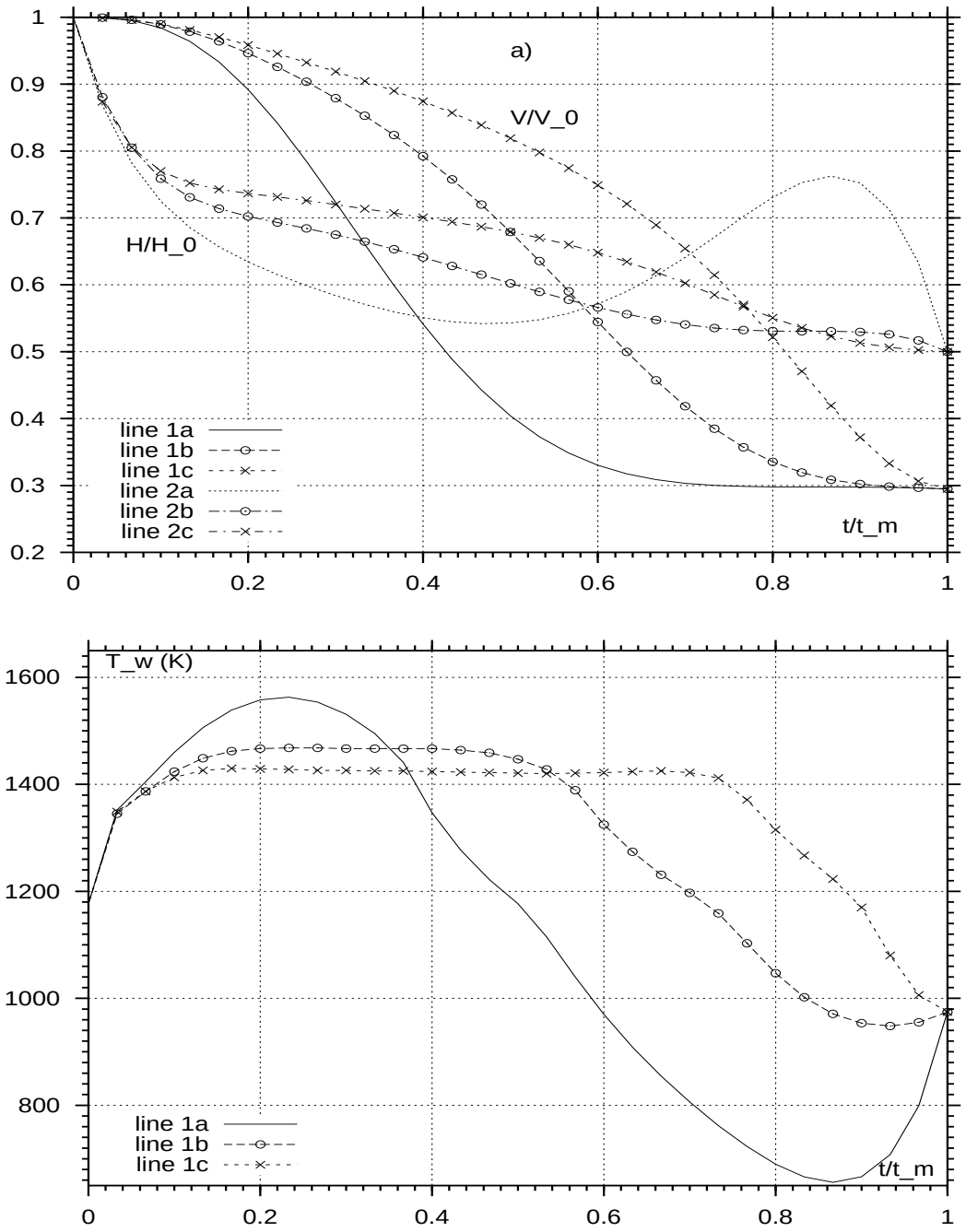

Figure 12: The distributions of temperature T_w versus τ (b), altitude H (lines 2) and velocity V (lines 1) versus τ (a) for various T_w^{max} and for $t_m = 15min$. $T_w^{max} = 2500K, 1548K, 1467K$ - lines a, b, c

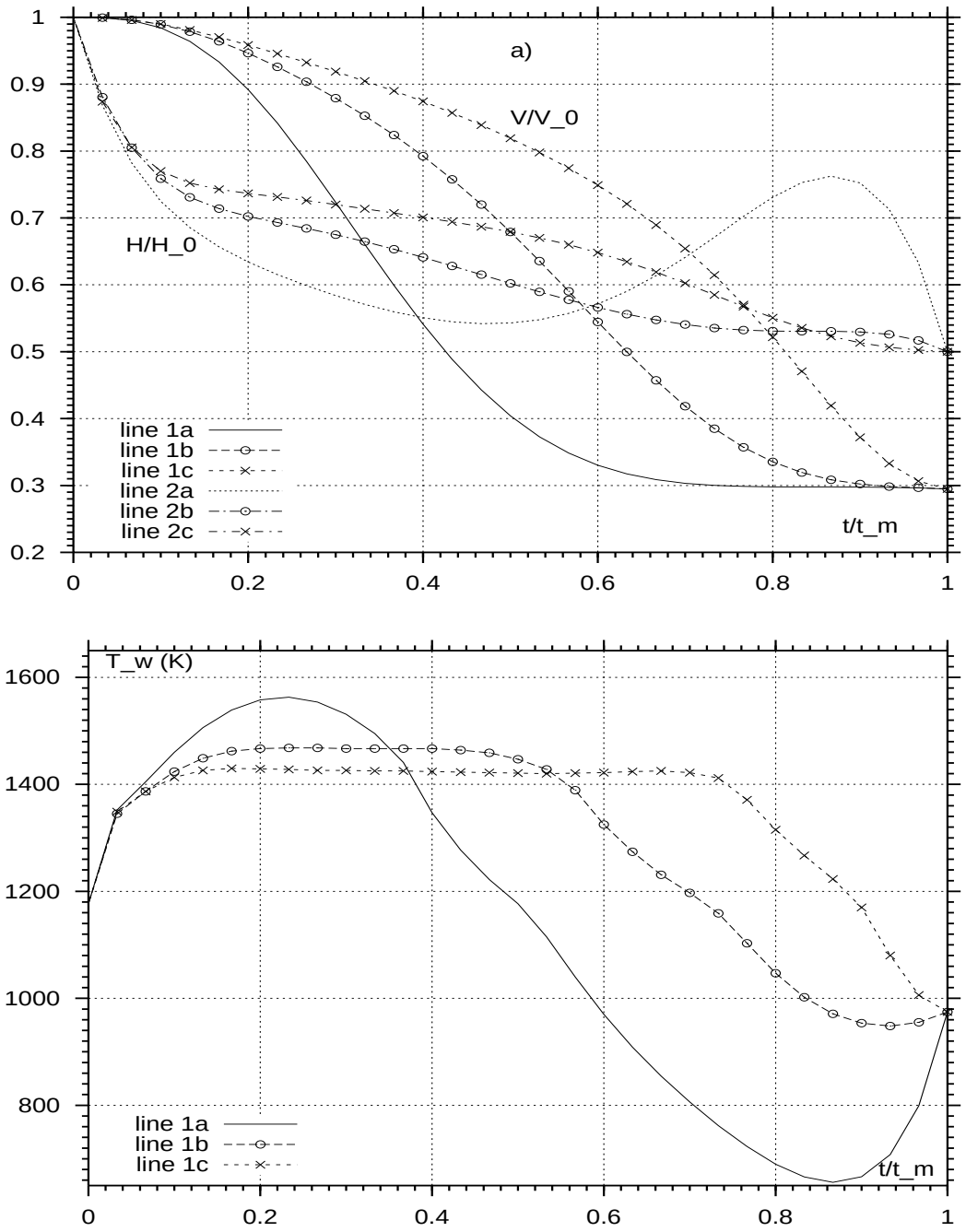

Figure 13: Distributions of temperature T_w versus τ (b), altitude H (lines 2) and velocity V (lines 1) versus τ (a) for various T_w^{max} and for $t_m = 15min$. $T_w^{max} = 2500K, 1470K, 1430K$ - lines a, b, c

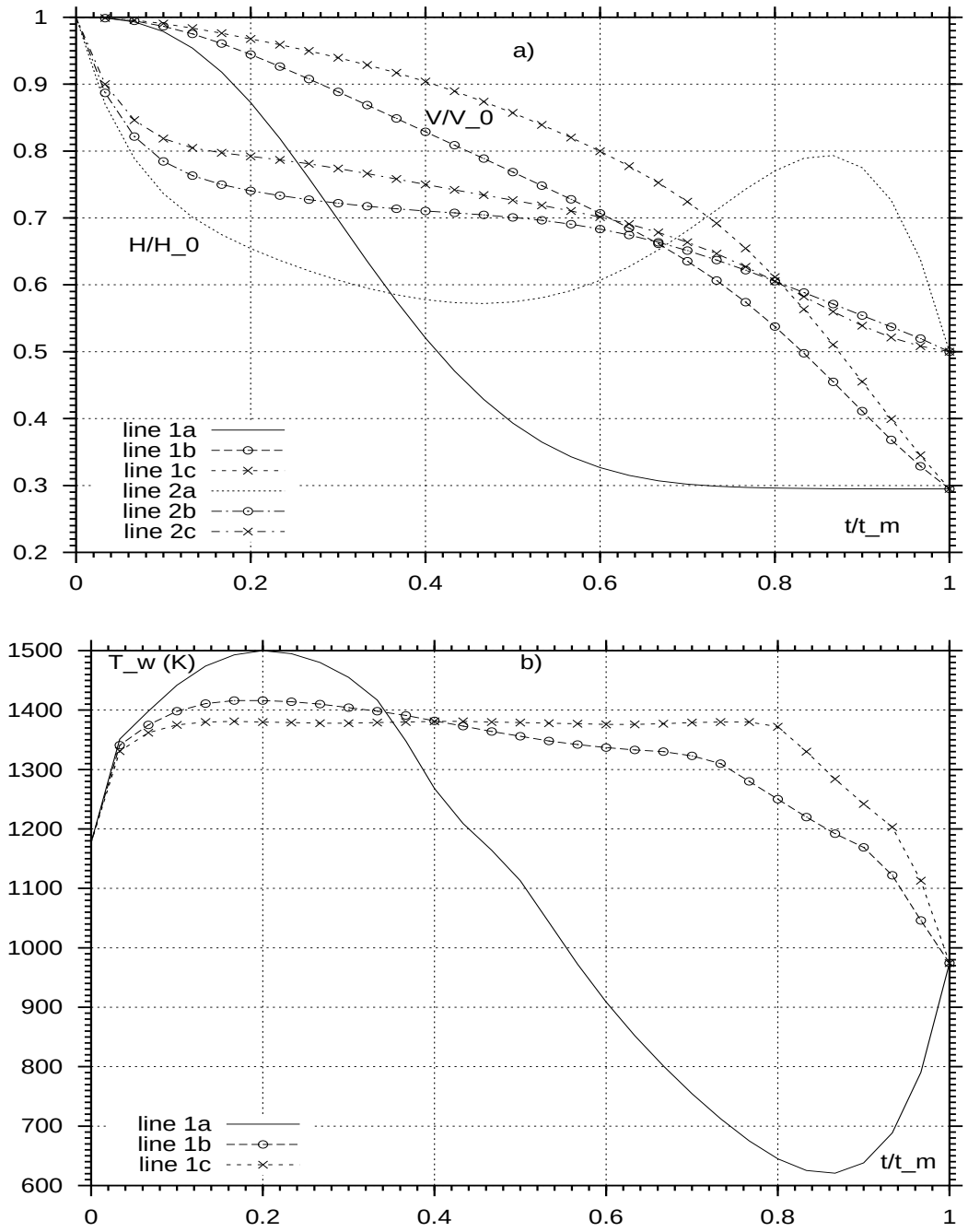

Figure 14: Distributions of temperature T_w versus τ (b), altitude H (lines 2) and velocity V (lines 1) versus τ (a) for various T_w^{max} and for $t_m = 30min$. $T_w^{max} = 2500K, 1416K, 1380K$ - lines a, b, c

low T_w^{max} value, because for all trajectories the maximum of the body surface temperature T_w will be exceed T_w^{max} and the problem constraint on T_w will be not satisfied.

In this case, it was interesting to consider the following minimax problem: find optimum trajectory with minimum integral heat flux and having minimum possible T_w^{max} value (named as minimax optimum trajectory). Some results of these calculations are presented in fig. 15-16. In fig.15 the distributions of temperature T_w versus τ (fig.15a) and altitude H versus velocity V (fig.15b) for minimax optimum trajectories and for various total flight time t_m are shown. In fig.16 the distributions of decelaration dV/dt (sm/s^2) along trajectory (fig.16a), altitude H/H_0 and velocity V/V_0 versus time τ (fig.16b) for minimax optimum trajectories and for different total flight time t_m are drawn. Lines a, b, c, d in fig.16 correspond to $t_m = 10min, 15min, 20min, 30min$; lines 1,2 in fig.16a correspond to maximum allowed drag deceleration along these trajectories and deceleration values realised along optimum trajectories.

The analysis of this minimax optimum trajectories demonstrated that for the opposite limit case (with possible low T_w^{max} value) a second non-monotonic flight altitude segment is absent.

From practical applications point of view it is very important to know how the optimal trajectory depends on the body geometry and on the rate of the heterogeneous chemical reactions proceeding at the body surface. Thus a number of calculations for various values of parameter k - ratio of the main curvatures of the body surface at the stagnation point (characterising body geometry) and for various catalytic activity of the body surface were carried out.

Some results of these calculations are shown in fig.17-19 where the the distributions of altitude H, of velocity V versus τ (fig.17a,18a,19a) and of temperature T_w versus τ (fig.17b,18b,19b) along various optimal trajectories for $k = 1.0, 0.2$ and for non-catalytic and ideal catalytic surface sre presented. In fig.17 ($t_m = 30min$) and in fig.18 ($t_m = 15min$) comparisons for non-catalytic surface and for $k = 1.0, 0.2$ are presented. Here lines a, c correspond to $k = 1.0$, lines b, d correspond to $k = 0.2$, lines a, b correspond to $T_w^{max} = 1500K$ (in fig.17) and to $T_w^{max} = 2500K$ (in fig.18), lines c, d correspond to minimax optimum trajectories: $T_w^{max} = 1380K$ for $k = 1.0$ and $T_w^{max} = 1268K$ for

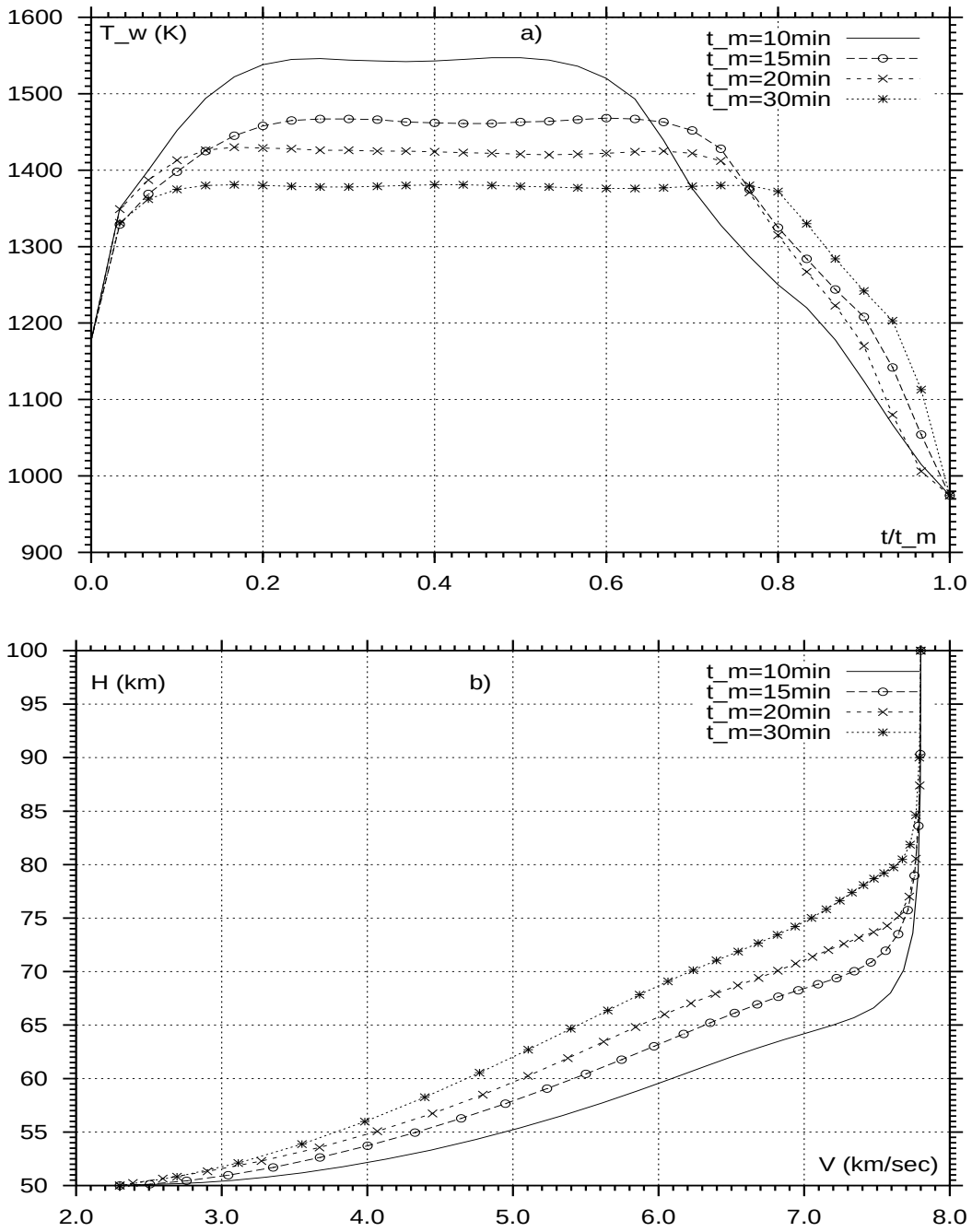

Figure 15: Distributions of temperature T_w versus τ (a) and altitude H versus velocity V (b) for minimax optimum trajectories and for different total flight times t_m.

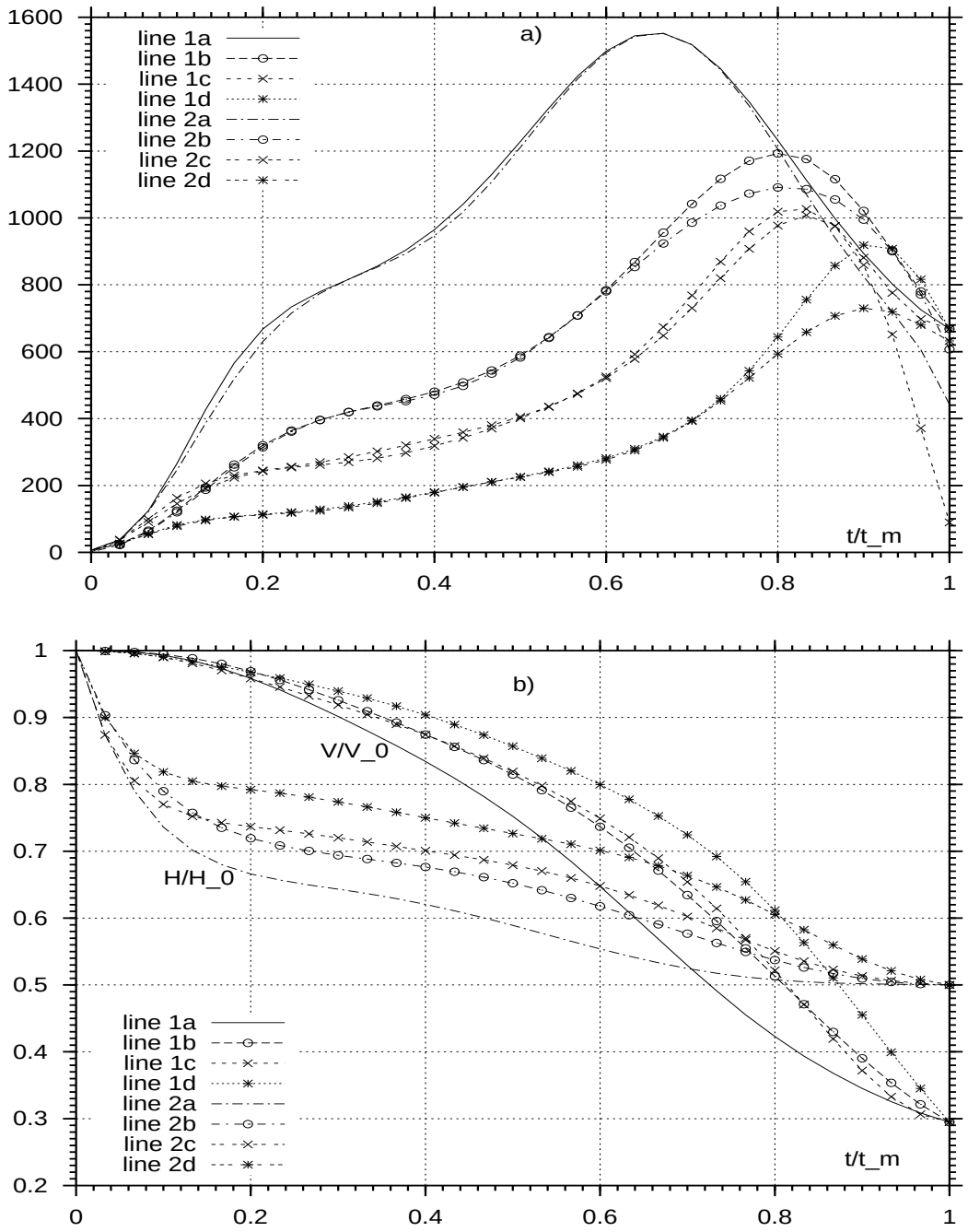

Figure 16: Distributions of deceleration dV/dt (sm/s^2) along trajectory (a),altitude H/H_0 and velocity V/V_0 versus time τ (b) for minimax optimum trajectories and for different total flight times t_m. Lines a, b, c, d correspond to $t_m = 10min, 15min, 20min, 30min$.

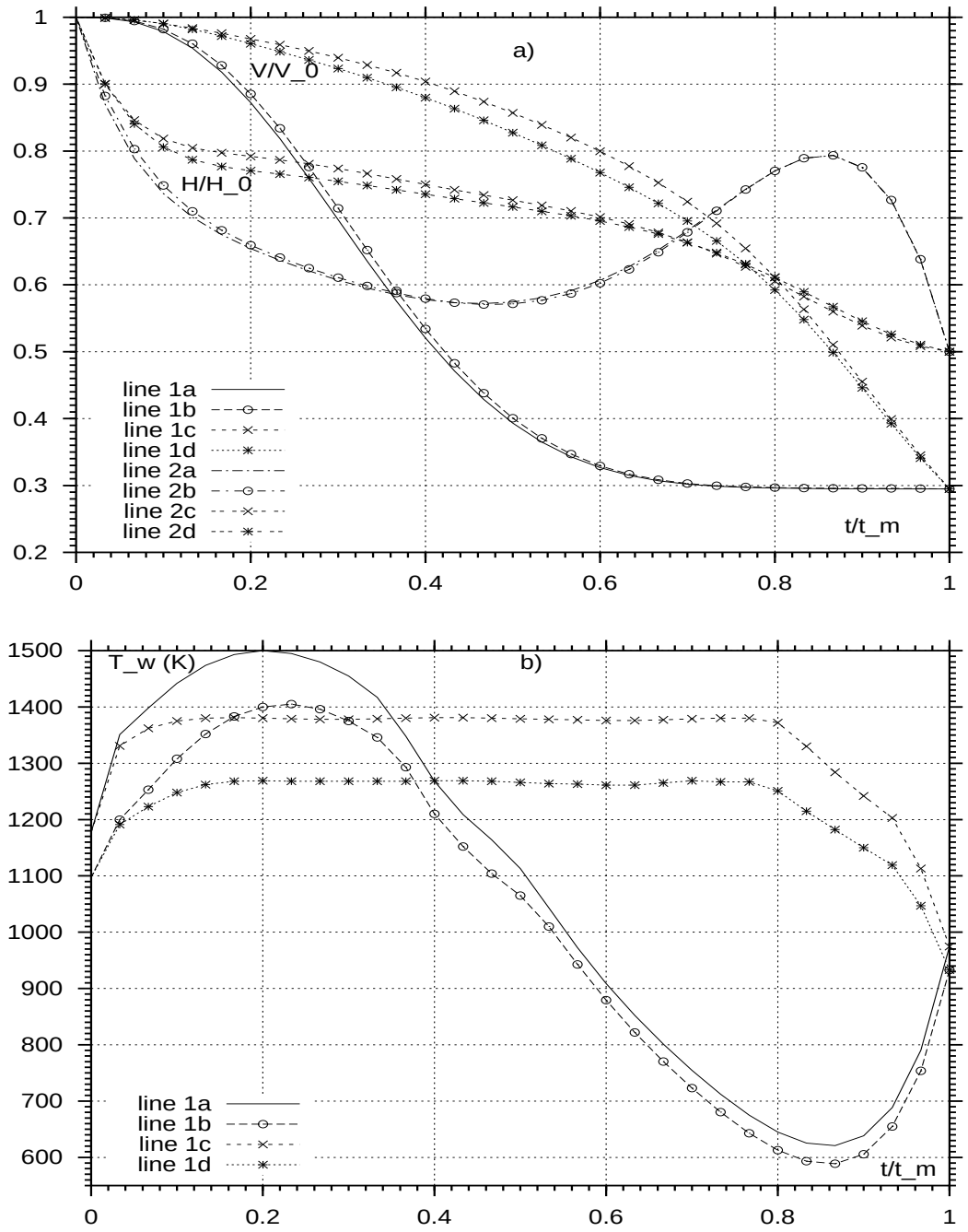

Figure 17: Influence of body geometry on optimal solutions for various T_w^{max} and for $t_m = 30min$. Lines a, c - $k = 1.0$, lines b, d - $k = 0.2$, lines a, b : $T_w^{max} = 1500K$, lines c, d : minimax optimum trajectories.

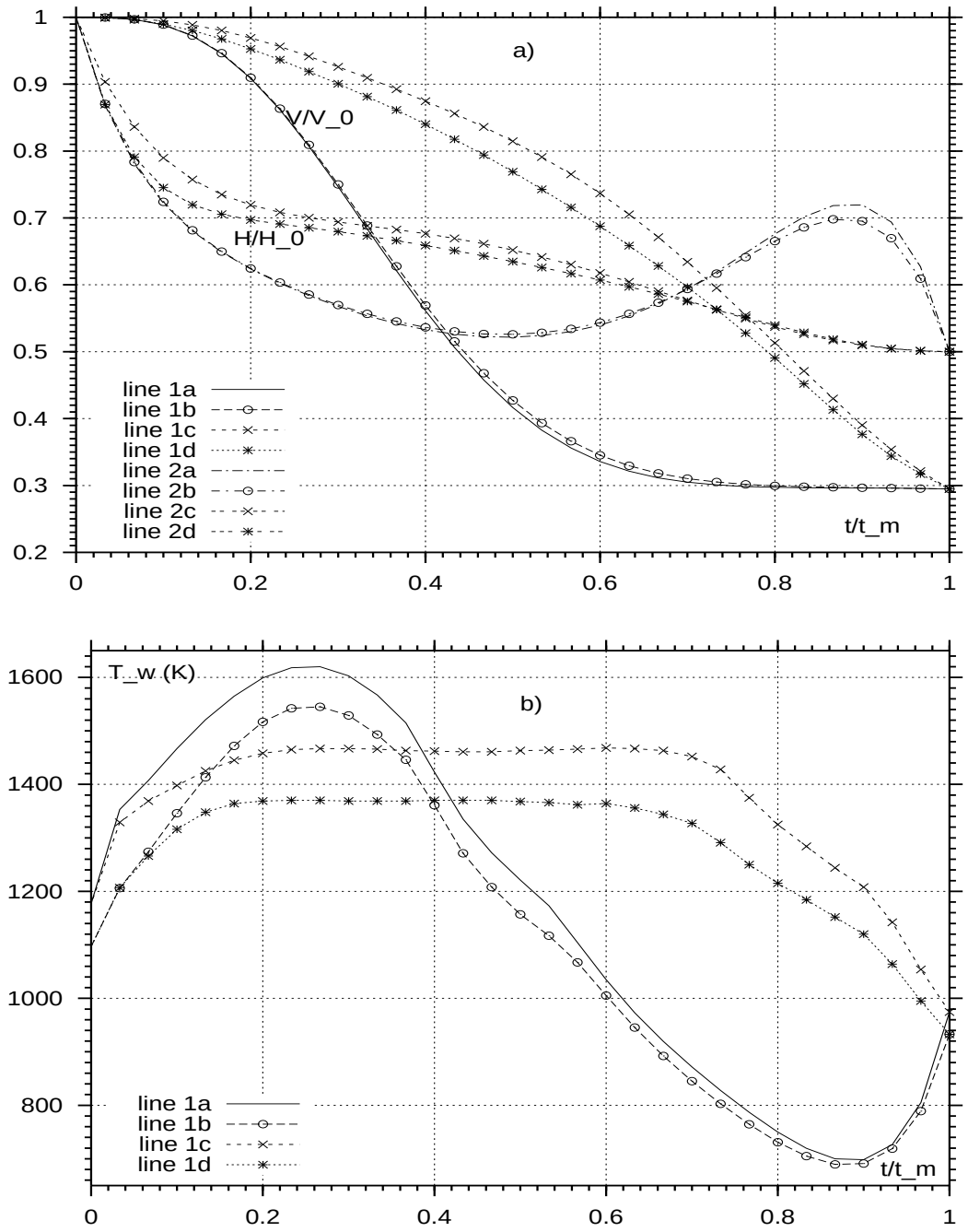

Figure 18: Influence of body geometry on optimal solutions for various T_w^{max} and for $t_m = 15min$. Lines a, c - $k = 1.0$, lines b, d - $k = 0.2$, lines a, b : $T_w^{max} = 2500K$, lines c, d : minimax optimum trajectories.

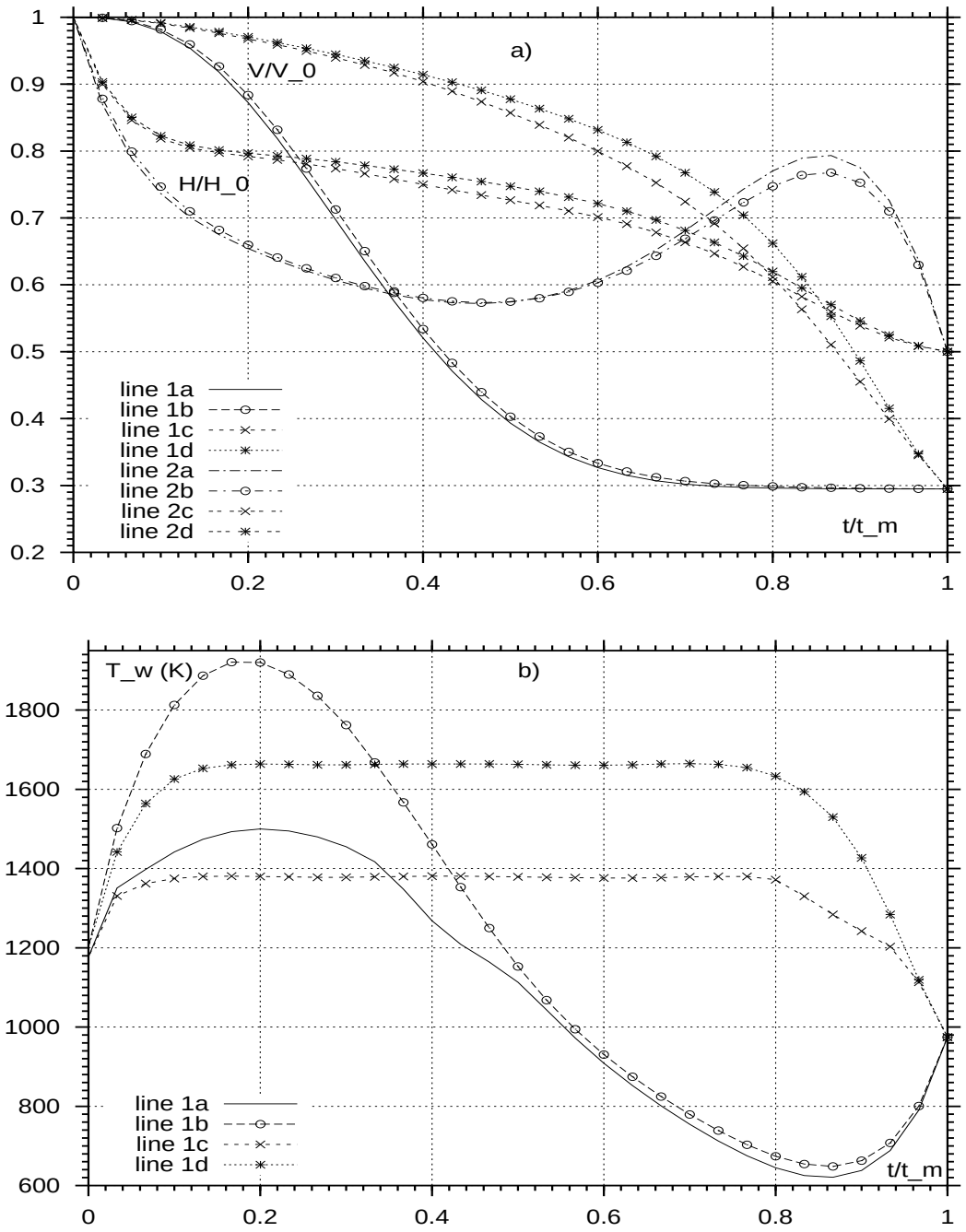

Figure 19: Influence of the catalytical activity of the body surface on optimal solutions for various T_w^{max} and for $t_m = 30min$. Lines a, c : non-catalytic surface, lines b, d : ideal catalytic one, lines a, b : $T_w^{max} = 2500K$, lines c, d : minimax optimum trajectories

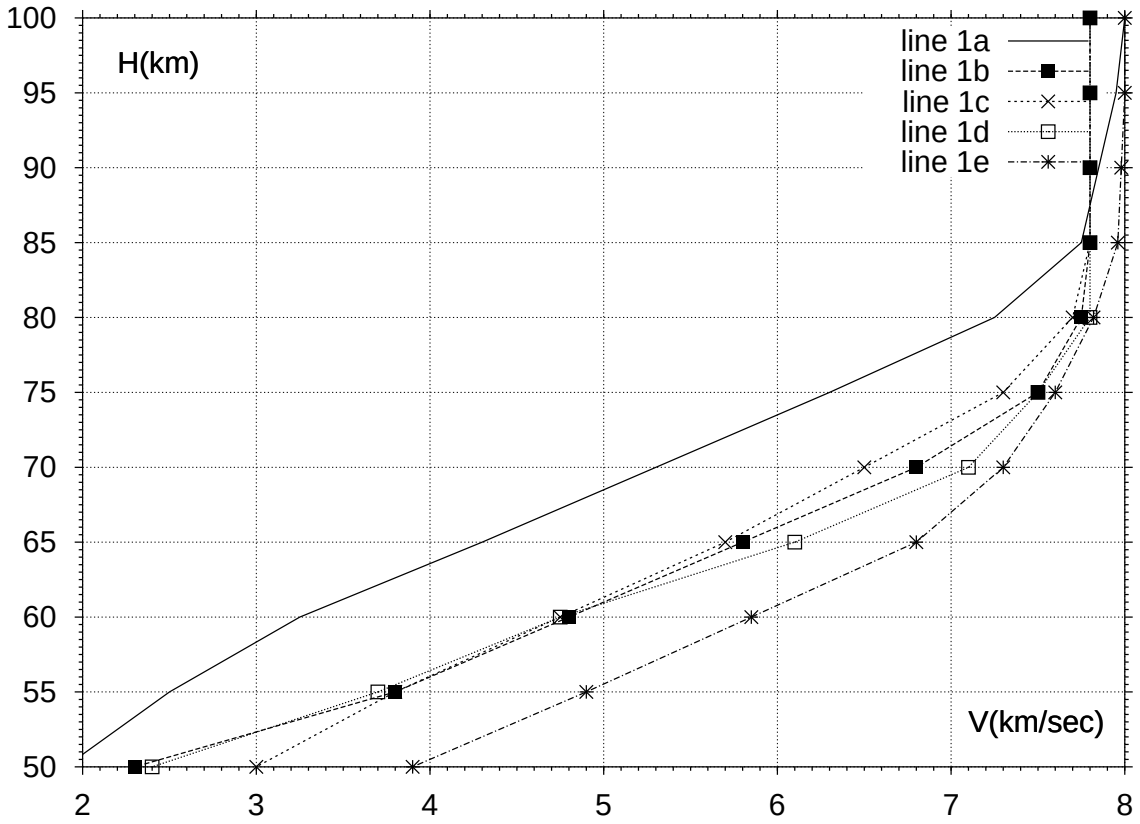

Figure 20: Comparison of the minimax optimum trajectory (line 1b) with "BURAN" trajectory (line 1d), with "SPACE SHUTTLE" trajectory (line 1c) and with the constant aerodynamic glide coefficient trajectories (lines 1a and 1e).

$k = 0.2$ (in fig.17); $T_w^{max} = 1467K$ for $k = 1.0$ and $T_w^{max} = 1370K$ for $k = 0.2$ (in fig.18).

Analogous comparisons between optimum solutions for non-catalytic surface and for ideal catalytic one are presented in fig.19 ($t_m = 30min$, $k = 1.0$). Here lines a, c correspond to non-catalytic surface, lines b, d correspond to ideal catalytic one, lines a, b correspond to $T_w^{max} = 2500K$, lines c, d correspond to minimax optimum trajectories: $T_w^{max} = 1467K$ for non-catalytic surface and $T_w^{max} = 1664K$ for for ideal catalytic one.

As it can be seen for all cases the influence of the body geometry and of the surface catalytic activity is rather low: for high T_w^{max} value the optimum trajectories practically coincide and for the opposite case the difference between minimax optimum trajectories is rather small also.

In conclusion let us present the comparison of the optimum trajectory with other known trajectories (fig. 20). Here line a, e correspond to the trajectory with the constant aerodynamic glide coefficient $10^{-3}m^2/n$ and $2 \cdot 10^{-4}m^2/n$ [16]; line b correspond to minimax optimum trajectory from this report line c is the "Space Shuttle" trajectory [13]; line d is the"Buran" trajectory [17]. It is seen that minimax optimum trajectory has very good correlation with the "Space Shuttle" and with the "buran" trajectory at the maximum heat flux domain.

References

[1] *Loicianskii L.G.* The laminar boundary layer. Fizmatgiz. Moscow. 1962.

[2] *Davis R.T.* Numerical solution of the hypersonic viscous shock-layer equations. AAIA Journal. 1970. V.8. No.5. P.843-851.

[3] *Cherny G.G.* Gas flow with hypersonic velocity. Fizmatgiz,Moscow (1959).

[4] *Peigin S.V.,Tirskii G.A. et al.* Super- and hypersonic aerodynamics and heat transfer. New-York. CRC Press. 1993.

[5] *Borodin A.I., Kazakov V.Yu., Peigin S.V.* Multicomponent 3D viscous shock layer solutions for blunt bodies with catalytic surface at angles of

attack and yaw. Izvestiya Acad. Nauk, Mechan. Zhidkosti i Gasa. 1990. No. 1. pp.143-150 (in Russian).

[6] Theory of optimum aerodynamic shapes. A.Miele(ed.) Academic press. London (1965)

[7] *Andrievskii V.V.* Dynamics of the space vehicle entry to Earth atmosphere. Moscow. Mashinostroenie, 1970, 232 p.

[8] *Hoffmeister F., Back T.* Genetic algorithms and evolution strategies: similarities and differences. In: Schefel H.P., Manner R.(eds.) Parallel Problem Solving from Nature - Proceedings of 1st Workshop. Dortmund. Germany. 1991. pp.455-469.

[9] *Michalewicz Z.* Genetic algorithms + data structures = evolution programs. New York. Springer-Verlag. Artificial Intelligence. 1992.

[10] *Sefioui M., Periaux J., Ganascia J.-G.* Fast convergence thanks to diversity. L.J.Fogel, P.J.Angeline and T.Back (eds). Evolutionary Programming V. Proc. of the 5th Annual Conference on Evolutionary Programming. MIT Press. 1996.

[11] *Peigin S.V.* Laminar boundary layer at the swirling flow over permeable surface. Izvestiya Akademii Nauk SSSR. Mekhanika Zhidkosti i Gasa. 1985. No. 6. pp.28-37.

[12] *Petukhov I.V.* Numerical calculation of two-dimentional flows in boundary layer. In: Chislennye metody resheniya differencialnyh i integralnyh uravnenii i kvadraturnye formuly. Nauka. Moscow. 1964 pp.304-325.

[13] *Masek R.V., Hender D., Forney J.A.* Evaluation of aerodynamic uncertainties for Space Shuttle. AIAA Paper. 1973. No.73-737.

[14] *Powers W.F.* A crude-search Davidon-type technique with application to shuttle optimization. AIAA Paper. 1972. No.72-907.

[15] *Agafonov V.P., Vertushkin V.K., Gladkov A.A., Polianskii Ä.Yu.* Nonequilibrium physical-chemical processes in aerodynamic. Mashinostroenie. Moscow, 1972.

[16] *Shkadov L.M., Bukhanova R.S., Illarionov V.F., Plokhih V.P.* Mechanics of optimal 3D motion of the aerodynamic vehicle at the atmosphere. Mashinostroenie. Moscow, 1972. 240 p.

[17] *Lozino-Lozinskii G.E.* The Buran flight. Gagarin's scientific conference on cosmonautics and aviation. Moscow. Nauka. 1990. pp.6-21.

Unité de recherche INRIA Sophia Antipolis
2004, route des Lucioles - B.P. 93 - 06902 Sophia Antipolis Cedex (France)

Unité de recherche INRIA Lorraine : Technopôle de Nancy-Brabois - Campus scientifique
615, rue du Jardin Botanique - B.P. 101 - 54602 Villers lès Nancy Cedex (France)
Unité de recherche INRIA Rennes : IRISA, Campus universitaire de Beaulieu - 35042 Rennes Cedex (France)
Unité de recherche INRIA Rhône-Alpes : 655, avenue de l'Europe - 38330 Montbonnot St Martin (France)
Unité de recherche INRIA Rocquencourt : Domaine de Voluceau - Rocquencourt - B.P. 105 - 78153 Le Chesnay Cedex (France)

Éditeur
INRIA - Domaine de Voluceau - Rocquencourt, B.P. 105 - 78153 Le Chesnay Cedex (France)
http://www.inria.fr
ISSN 0249-6399